European Journal of Neuroscience, Vol. 26, pp. 1950–1968, 2007 doi:10.1111/j.1460-9568.2007.05783.x

Directional responses of visual wulst neurones to grating and plaid patterns in the awake owl

Jerome Baron,[1] Lucas Pinto,[1] Marcelo Oliveira Dias,[1] Bruss Lima[2] and Sergio Neuenschwander[2]
[1]Department of Physiology and Biophysics, Institute of Biological Sciences, Federal University of Minas Gerais, Av. Antonio Carlos 6627, Belo Horizonte, MG 31270-901, Brazil
[2]Max-Planck Institute for Brain Research, Frankfurt am Main, Germany

Keywords: burrowing owl, evolution, motion integration, visual forebrain

Abstract

The avian retinothalamofugal pathway reaches the telencephalon in an area known as visual wulst. A close functional analogy between this area and the early visual cortex of mammals has been established in owls. The goal of the present study was to assess quantitatively the directional selectivity and motion integration capability of visual wulst neurones, aspects that have not been previously investigated. We recorded extracellularly from a total of 101 cells in awake burrowing owls. From this sample, 88% of the units exhibited modulated directional responses to sinusoidal gratings, with a mean direction index of 0.74 ± 0.03 and tuning bandwidth of 28 ± 1.16°. A direction index higher than 0.5 was observed in 66% of the cells, thereby qualifying them as direction selective. Motion integration was tested with moving plaids, made by adding two sinusoidal gratings of different orientations. We found that 80% of direction-selective cells responded optimally to the motion direction of the component gratings, whereas none responded to the global motion of plaids, whose direction was intermediate to that of the gratings. The remaining 20% were unclassifiable. The strength of component motion selectivity rapidly increased over a 200 ms period following stimulus onset, maintaining a relatively sustained profile thereafter. Overall, our data suggest that, as in the mammalian primary visual cortex, the visual wulst neurones of owls signal the local orientated features of a moving object. How and where these potentially ambiguous signals are integrated in the owl brain might be important for understanding the mechanisms underlying global motion perception.

Introduction

Many neurones in the primary visual cortex (V1) of carnivores and primates exhibit some degree of directional selectivity (Hubel & Wiesel, 1962, 1968). Although these neurones are presumed to be important for mediating motion perception, their individual contribution to this process is potentially ambiguous. Indeed, receptive fields in V1 are small, meaning that most contours constituting an object will extend outside the suprathreshold response area of a cell. Ambiguities may thus arise as a cell's preferred direction, orthogonal to a contour's orientation (Henry *et al.*, 1974; Schiller *et al.*, 1976), might not be the same as the direction of the whole object. These ambiguities, commonly referred to as the aperture problem, somehow need to be overcome in order to recover an object's correct trajectory (Wallach, 1935; Fennema & Thompson, 1979; Marr & Ullman, 1981). Cortical models have traditionally favoured a hierarchically organized two-stage process whereby several local motion signals available in V1 are disambiguated by binding operations taking place in higher motion-specific areas (Movshon *et al.*, 1985). However, how such binding operations are exactly accomplished and whether they are actually at all necessary remain unclear (van Wezel & van der Smagt, 2003; Singer, 2004; Majaj *et al.*, 2007).

With the aim of providing comparative insights into this issue, we have here assessed whether neurones in the visual wulst of the owl are capable of signalling global motion. The visual wulst is the telencephalic recipient of the avian retinothalamofugal pathway (Shimizu & Bowers, 1999). In owls, this structure is particularly developed (Stingelin, 1958; Iwaniuk & Hurd, 2005; Iwaniuk & Wylie, 2006) and, like V1, it contains neurones that have small retinotopically organized receptive fields, a high degree of binocular integration, selectivity for orientation and motion direction, and binocular disparity tuning (Pettigrew & Konishi, 1976; Pettigrew, 1979; Wagner & Frost, 1993, 1994; Nieder & Wagner, 2000, 2001a,b). Such response properties would suggest that the aperture problem is present at the level of the visual wulst but this remains speculative because the available information about directional selectivity is limited and of qualitative nature. Moreover, some physiological features of the wulst are known to resemble more closely those found in extrastriate areas (Pettigrew, 1979; Wagner & Frost, 1994; Nieder & Wagner, 1999; Liu & Pettigrew, 2003), leaving open the possibility that motion integration occurs at an early level in the owl.

Our approach relied on a now classical paradigm, introduced by Movshon *et al.* (1985) for studying motion integration. This paradigm uses plaid patterns, consisting of two superposed, non-parallel gratings, in order to classify cells on the basis of whether they respond preferentially to the motion of each component grating or to the motion of the plaid as a whole. In our study, we found that most visual wulst neurones respond selectively to the individual component gratings and thus do not signal the global motion of the plaids. Parts of these results have been reported in abstract form (Pinto *et al.*, 2006, 2007).

Correspondence: Dr Jerome Baron, as above.
E-mail: jbaron@icb.ufmg.br

Received 20 May 2007, revised 17 July 2007, accepted 24 July 2007

Materials and methods

Animal training

Experiments were performed on five adult burrowing owls (*Athena cunicularia*), weighing between about 160 and 190 g. Burrowing owls are small, long-legged owls, residents of open dry grasslands and desert habitats, and are very common in south-eastern Brazil. They are highly visual animals and have a marked fovea (Bravo & Pettigrew, 1981). Unlike most owls, they are active during the day (Coulombe, 1971) and lack the prominent facial disks that facilitate nocturnal owls in locating prey by sound (Norberg, 1977; Konishi, 1993). The animals that took part in the present experiments were housed in spacious outdoor aviaries together with the rest of the owl colony that we maintain in our laboratory under licence from the Brazilian Institute for the Environment and Natural Renewable Resources (IBAMA, licence no. 02015.004197/03).

Extracellular recordings from awake, passively fixating burrowing owls were obtained by following a method recently developed by our group. At this point, it is important to highlight that, in owls, passive fixation can be achieved by head fixation only, owing to the fact that eye movements are extremely limited in these birds (Steinbach *et al.*, 1974; Pettigrew & Konishi, 1976; Knudsen, 1982) reaching, in the burrowing owl, a maximum amplitude of 0.5° (Cooper & Pettigrew, 1979). Our approach was therefore to train owls to tolerate body restraint and rigid head fixation for periods long enough to accommodate cell recordings. Training initially began by taming the owls, handling them daily during a period of approximately 4 weeks. Using standard falconry techniques, the animals were carried around as much as possible to get them used to all sights and sounds of the laboratory. In particular, the birds were left to explore the recording booth. Following this initial taming period, the owls underwent surgery for the implantation of a recording chamber, as detailed below. After a minimum of 4 days of recovery, the owls were then trained to get used to head fixation. Positive reinforcement in the form of small pieces of meat was used and handling was executed with as much calm as possible in order to avoid conditioning of aversive responses. Owls were accustomed to wearing a leather jacket and being secured onto a perch by wrapping Velcro® straps around their claws. After about 1 week, head restraint was introduced and quickly combined with electrophysiological recordings. Installation into the head-fixation apparatus was fast and relatively stress-free for the animals. Once secured, and provided that no brusque movements were made around them, the owls typically remained in a state of quiet wakefulness for progressively longer periods. Thereafter, they often began to fidget or show signs of tiredness and, as soon as this was detected, the session was interrupted. Periods of head fixation were limited to about 3–4 h and their effect on animal welfare was closely monitored during and between recording sessions.

All procedures used in the present work were approved by the Ethics Committee for Animal Experimentation (CETEA, licence no. 2004/01) of the Federal University of Minas Gerais and were conducted in accordance with the European Communities Council Directive of 24 November 1986 (86/609/EEC).

Surgical procedures

A lightweight recording chamber was surgically mounted over the cranial area above the visual wulst. In addition to providing access to the brain, this chamber was used to fix the head of the animal during the recordings. It consisted of a single cylindrical metal piece (1.5 mm thick and 8 mm high) with a 10 mm internal diameter and weighing 1 g. For surgery, anaesthesia was induced and maintained with Zoletil® 50 (1 : 1 mixture of tiletamine and zolazepam, Virbac, Carros, France) administered in the pectoral muscle at a dose of 20 mg/kg (half doses for maintenance). After loss of reflexes, the animal was wrapped into a leather jacket and its head was fixed into a stereotaxic frame (model 1430, David Kopf Instruments, Tujunga, CA, USA). To expose the surface of the skull, the skin was incised 25–30 mm along the midline and retracted laterally. The position of the craniotomy was marked out on the skull according to stereotaxic coordinates preliminarily worked out in our laboratory to target the visual wulst in the middle of its anterior/posterior dimension and proximate to its lateral margin, adjacent to the vallecula. This region corresponds to the foveal and parafoveal representations in the visuotopic map described in the wulst by Pettigrew (1979). The recording chamber was centred over this stereotaxic reference point and cemented to the skull in an upright position such that electrode penetrations could be roughly made perpendicular to the wulst. Care was taken to ensure that the dental cement (Vitro Fil®, DFL, Rio de Janeiro, RJ, Brazil) could also make its way into the spongious bone cavities exposed at various sites around the cylinder. This provided strong adherence of the cement to the cranium. After suturing the midline incision around the cylinder, a circular craniotomy (about 3 mm in diameter) was then made. Surgery took approximately 1 h and antiseptic conditions were maintained throughout. A broad-spectrum antibiotic (50 mg/kg of Terramicine®, Pfizer Laboratories, São Paulo, SP, Brazil) as well as an analgesic/anti-inflammatory (2 mg/kg of Ketofen® 1%, Merial, São Paulo, SP, Brazil) were administered post-operatively by intramuscular injections.

Recordings

Spiking activity was recorded from individual neurones or small groups of neurones using quartz-insulated platinum/tungsten electrodes (Thomas Recording, Giessen, Germany) with an impedance of 0.3–0.8 MΩ at 1 kHz. Signals were amplified (× 1000) and band-pass filtered between 300 Hz and 7 kHz (HST/16o25 headset, 32-channel pre-amplifier box, Plexon, Dallas, TX, USA) before being digitized at 32 kHz by a high-speed, 16-bit resolution A/D card with onboard trigger and timer capabilities (PCI-6259, National Instruments, Austin, TX, USA). The A/D board was also programmed to provide a second amplification stage of ×10. Signal display, acquisition and storage were controlled through custom software written in LABVIEW (National Instruments) hosted in a 2 GHz AMD Athlon PC.

For independent positioning of the electrodes, we have developed, at the Max-Planck Institute, a recording device that consists essentially of three precision hydraulic microdrives mounted onto an X/Y stage (MO95, Narishige Scientific Instrument Laboratory, Tokyo, Japan). Each electrode was back-loaded into a guide tube and connected to a single microdrive. The device was secured to the recording chamber via a coupling ring adapter screwed on top of the chamber by means of a thread made inside it. The same thread was also used for fastening a protective cap when no recordings were made. The recording device was held in place by a metallic arm and this ensemble provided sufficient rigidity to fixate the head of the animal. With such an arrangement, negligible relative movements occurred between the electrodes and the head of the animal and good recording stability was therefore obtained. The relative positions of penetrations were defined by pre-set coordinates from the X/Y stage. These coordinates were varied across recording sessions in order to sample as many sites as possible. The electrodes were lowered inside their protecting guide tubes until contact with the dura was signalled by a characteristic noise in the recorded signal. The search for neurones was based on the

quality of unit signals, not responsiveness. Cells isolated along the same track were spaced at 200 μm intervals or greater. In some penetrations, the first 1000 μm were ignored so that sampling biases across the different layers of the wulst could be minimized.

Only spikes exceeding a pre-set threshold were detected, and saved, together with their time of occurrence. This detection threshold was set as a multiple of the SD of the whole voltage trace. We typically used thresholds between 2 and 3 SDs. Single unit activity was determined on the basis of the constant amplitude and shape of the extracted waveforms, using several online sorting tools available in our software.

Unit isolation was further refined offline by using spike-sorting software developed at the Max-Planck Institute for Brain Research by Nan-Hui Chen. This program uses a semiautomatic clustering procedure based on a dynamic template-matching algorithm. The estimation of the number of units present, as well as the assignment of each spike to a unit, was based on a conventional distance metric (residual sum of squares) between a spike and a template. Based on this distance, a similarity index threshold was calculated to decide how many units were present and if a spike should be assigned to a particular template or to noise. Threshold setting was dynamically computed by an artificial neural network based on the Adaptive Resonance Theory (Carpenter & Grossberg, 1987). Sorting was initiated by leaving the template-matching algorithm to find as many clusters as possible automatically. We then switched to a manual mode in which the experimenter could decide which clusters to merge, if any. Numerous graphical and analytical tools, such as the refractory period seen in the auto-correlogram, were available to guide this decision. A change in waveform amplitude over time was also computed and displayed for each cluster to identify and reject any single units with significant instability during a recording session. Correct spike assignment was validated if distinct clusters could be seen in two- and three-dimensional plots of spike principal-component-analysis scores, and if the overall separation of these clusters could be confirmed by objective measurements provided by the J3 and Pseudo-F statistics [more details on how these values are calculated can be found in Spath (1980) and Wheeler (1999)].

Overall, a yield of one unit per recording electrode was the most frequent outcome of the aforementioned analysis. Only occasionally could two, and rarely up to three, units per electrode be confidently isolated. Not only the numbers of offline-isolated units per electrode but also the response profile of such units were globally coherent with prior online estimation. These considerations, combined with the fairly stringent criteria adopted for offline sorting, made us confident that only well-isolated units were considered for the analysis described below.

Stimulation protocol

Visual stimuli were displayed on a 19-inch RGB video monitor (Samsung SyncMaster 955DF) at a resolution of 1024 × 768 pixels and a video frame rate of 100 Hz. The video monitor was placed 57 cm from the owl's eye and, at this distance, the usable part of the screen subtended 27 × 36° of visual angle. Using custom software written in LABVIEW (National Instruments), stimuli were prepared as sequences of bitmap images, which were then presented with timing accuracy as movies by the ACTIVESTIM software (http://www.activestim.com).

Once a cell was isolated, its receptive field was plotted on the screen as a minimum response field (Barlow *et al.*, 1967) by listening to neuronal discharges and presenting mouse-controlled objects such as spots, bars, checkboards and so forth. Ocular dominance and optimal orientation/direction of motion were also determined in a similar way. If any doubts were cast upon the reliability of this qualitative evaluation, all of the above response properties were reassessed quantitatively. This was done mainly by analysing a two-dimensional spatial map of neuronal responsiveness derived from a stimulation protocol in which a single bar (10° in length and 0.5° in width) was swept across the screen in 16 different orientations (Azzi, 2004). Following this preliminary assessment, all receptive field measurements were then made: (i) through the eye that more effectively activated the cell (the non-dominant eye was covered) and (ii) with the centre of the receptive field roughly at the centre of the monitor screen. We usually assessed the preferences of the neurone for spatial and temporal frequency, either qualitatively or quantitatively. Such evaluation was performed by analysing the cell responses to a full-contrast drifting sine-wave grating, optimized for direction, and presented in varying spatial and temporal frequencies inside the receptive field. We did not attempt to control for eye movements because, as previously mentioned, such movements are very limited in owls.

Our primary goal in this study was to compare the selectivity of visual wulst neurones to the direction of motion of grating and plaid patterns, and for this we used a stimulation protocol fairly similar to those used by previous related studies in mammals (see for example Gizzi *et al.*, 1990; Movshon & Newsome, 1996; Guo *et al.*, 2004). All visual stimuli were made to appear within a circular aperture of 10° diameter that was aligned with the centre of the receptive field. Conventional sine-wave gratings were used. Their spatial and temporal frequencies were optimized according to preliminarily established values and their Michelson contrast was set to 0.45. Plaids were obtained by adding two such gratings separated by 90 or 135° in orientation (plaid mean luminance 35.1 cd/m^2). Both grating and plaid stimuli were presented over 360° in 16 steps of 22.5°. As the same 16 directions were used for all tests on all neurones, a total of 32 different stimulus conditions were shown. Each stimulus appeared for 10 trials on a pseudorandom schedule to counter repetition effects. In a trial, a stimulus was presented for 2 s, immediately preceded and followed by 500 ms periods of blank, during which a homogeneous grey field with the same mean luminance as that of the stimulus was shown. An interstimulus interval of 2 s was introduced to minimize potential interactions between the sequential stimuli. With 10 repeated presentations for each condition, the stimulus protocol required about 25 min to complete.

When referring to the motion direction of grating and plaid patterns, we used the following conventions: a grating with vertically orientated stripes moving rightwards was considered to have a direction of motion of 0°, whereas a grating with horizontally orientated stripes moving upwards was considered to have a direction of 90°. The drift direction of a plaid was referenced by the same polar coordinate system as that adopted for gratings and was defined as the direction of global motion perceived by a human observer. For the type of plaids used in this study, this corresponds to a direction of motion that lies equidistant between the directions of the two component gratings.

Data analysis

Data were initially screened with peristimulus time histograms and raster plots. The measure of neuronal response used for comparing the effects of different stimulus conditions was the mean spike rate computed within a specific time window. For the main part of the analysis, a window of 1800 ms, starting 200 ms after stimulus onset, was chosen to calculate the mean evoked response. By excluding the

first 200 ms of stimulus presentation, we sought to minimize the eventual contribution of onset components not directly related to the motion direction of the drifting pattern. In the final part of the Results, we perform an additional analysis on this initial 200 ms period in order to assess the direction of motion selectivity in the earliest phase of responses. Spontaneous activity was calculated as the mean spike rate across all stimulus conditions measured 500 ms before stimulus onset, which corresponded to the initial blank periods with no stimuli present on the monitor screen.

The attribution of directional selectivity to a particular cell was based on a combination of statistical and threshold-based criteria, which were applied on cell responses to drifting sinusoidal gratings, plotted on a linear scale or in a polar coordinate system as a function of motion direction (direction tuning curves). First, we made sure that each neurone considered for further analysis had significantly stronger evoked responses than its mean spontaneous activity when it was stimulated with gratings of optimal direction of motion. This was done by comparing, for this particular condition, the firing frequency in a 500 ms window immediately before and after stimulus onset using the one-tailed Wilcoxon matched-pairs signed-rank test ($P < 0.05$). Following well-established conventions, the motion direction for which the response was significantly greater than both the spontaneous activity and all other data points in the tuning curve was formally defined as the preferred direction. The direction 180° away from the preferred direction was defined as the antipreferred direction. Next, we performed an ANOVA using direction of motion as the main factor and a criterion of $P < 0.05$ to determine whether there was a statistically significant relationship between firing rate and motion direction. Depending on the normality of the sampled mean responses (Lilliefors test, $P < 0.05$, see the *General statistics* section below), this statistical analysis was carried out using either ANOVA or its non-parametric analogue, namely the Kruskal–Wallis test. Cells that yielded non-significant terms in ANOVA were considered as omnidirectional and excluded from our data set. For the remainder, a direction index (DI) was calculated as:

$$\mathrm{DI} = 1 - [(R_{\mathrm{anti}} - R_{\mathrm{spont}})/(R_{\mathrm{pref}} - R_{\mathrm{spont}})]$$

where R_{pref} and R_{anti}, respectively, represent the responses to motion in the preferred and antipreferred directions relative to the spontaneous activity (R_{spont}). DI values increase from 0, for cells equally responsive to both directions, to 1, for cells that respond exclusively to one direction of motion, and can be greater than 1 if the cell responds below spontaneous activity levels for motion in the antipreferred direction. Cells with a DI ≥ 0.5 were considered as direction selective and only these were further analysed with respect to their selectivity for the direction of motion of plaid patterns. Cells with a DI < 0.5 were referred to as non-direction selective.

The width of direction tuning was calculated by first fitting parametric curves to neuronal responses as a function of the direction of grating motion and then by taking the half-width at half-maximum of the fitted curves. All fits were based on the probability density function of the von Mises distribution, which is the circular statistics analogue of the normal distribution. As proposed by Swindale *et al.* (2003), we used the sum of two von Mises functions for cells that exhibited a visible peak in the antipreferred direction. In this case, the fitting parametric curve was:

$$M(\phi) = m + A_1 e^{[k_1(\cos(\phi-\phi_1)-1)]} + A_2 e^{[k_2(\cos(\phi-\phi_2)-1)]}$$

In the above expression, ϕ is the grating direction of motion for which the response is being estimated and m, A_1, A_2, ϕ_1, ϕ_2, k_1 and k_2 are free parameters. m corresponds to the baseline level. The parameters A_1 and A_2 represent the maximum heights of the individual peaks, ϕ_1 and ϕ_2 are the centre directions (in radians) of each peak, and k_1 and k_2, known as concentration factors, are inversely related to the widths of each peak. For cells with no visible peaks in the antipreferred direction, A_2 was constrained to equal 0, which removed the second von Mises function from the above equation. All of the parameters were adjusted by an iterative least-square fitting method, using the trust region for non-linear minimization algorithm (Branch *et al.*, 1999) available in the Matlab Curve Fitting Toolbox (MathWorks, Natick, MA, USA). As initial values, we used the following: A_1 = the maximum value of the data, $A_2 = 0.7\ A_1$, $k_1 = k_2 = 2.0$ (corresponding to a bandwidth of 50°) and $\phi_2 = \phi_1 + 180°$. Fits that accounted for less than 80% of the variance, as determined by the R^2 statistics, were rejected.

To assess whether the directional selectivity of visual wulst neurones was better described as component (CDS) or pattern (PDS) direction selective, we used a revised version (Rodman & Albright, 1989; Movshon & Newsome, 1996) of the partial correlation analysis introduced by Movshon *et al.* (1985). Essentially, this analysis involved comparing the response of each neurone to the plaid pattern with the predictions of idealized models of pattern and component direction selectivity. Both modelled predictions were generated from the response of the neurone to the drifting grating. The predicted response for the pattern model was identical to the grating tuning curve. The predicted response for the component model was generated by taking the sum of two grating tuning curves, each shifted by ±45° for 90° plaid angles or ±67.5° for 135° plaid angles. For this latter prediction, spontaneous activity was subtracted from the response to the grating and added back after the prediction had been computed. To control for potential non-independence of the two model predictions, the degree of similarity between the actual plaid tuning curve and the predicted tuning curves for pattern and component direction selectivity was quantified by two partial correlation coefficients:

$$R_{\mathrm{p}} = (r_{\mathrm{p}} - r_{\mathrm{c}} r_{\mathrm{pc}})/\sqrt{[(1 - r_{\mathrm{c}}^2)(1 - r_{\mathrm{pc}}^2)]}$$

$$R_{\mathrm{c}} = (r_{\mathrm{c}} - r_{\mathrm{p}} r_{\mathrm{pc}})/\sqrt{[(1 - r_{\mathrm{p}}^2)(1 - r_{\mathrm{pc}}^2)]},$$

where R_{p} is the partial correlation coefficient for the pattern prediction, R_{c} is the partial correlation coefficient for the component prediction, r_{c} is the Pearson's linear correlation coefficient between the response to plaids and the model prediction for an idealized component neurone, r_{p} is the linear correlation coefficient between the response to plaids and the modelled pattern neurone response, and r_{pc} is the linear correlation coefficient between the two modelled predictions.

The statistical significance of R_{p} and R_{c} was determined by a parametric statistical value, t, calculated first by converting both partial correlation coefficients (R_x, with x = p and c) into Z-scores (Z_x) using Fisher's r-to-Z transformation (Papoulis, 1990):

$$\mathrm{Z}_x = 0.5 \times \ln[(1 + R_x)/(1 - R_x)]$$

and then by computing the difference between the Z-scores as follows:

$$t = (\mathrm{Z}_p - \mathrm{Z}_c)/\sqrt{(2/DoF)}$$

In this equation, *DoF* refers to the degrees of freedom and is equal to the number of conditions used to measure directional tuning curves minus three (in our study $DoF = 13$, as 16 directions were used for measuring tuning curves). As in previous related studies, a conditional

probability of $P = 0.1$ was chosen as the significance threshold for R_p and R_c. The reason for choosing this non-conservative criterion is that the present statistical procedure is not a true test for significance but is expected to adequately reduce the data (Movshon *et al.*, 1985; Gizzi *et al.*, 1990; Scannell *et al.*, 1996). Accordingly, for a cell to be classified as a PDS cell, R_p had to be significantly greater than either R_c or zero. Similarly, R_c had to exceed R_p or zero above chance level, for a cell to be classified as CDS. If a cell met neither of these criteria, it was considered unclassified.

To get an idea of the relative strength between component-like selectivity and pattern-like selectivity expressed by each neurone in response to plaid patterns, we computed a component index defined as $R_c^2 - R_p^2$ (Stoner & Albright, 1992; Pack *et al.*, 2001; Guo *et al.*, 2004). R_c^2 and R_p^2 are effectively the variance accounted for by the component and pattern predictions, respectively.

General statistics

In addition to the partial correlation analysis, several standard statistical tests were also computed. Before datasets were compared, we used the Lilliefors modification of the Kolmogorov-Smirnov test to check whether the datasets in question were significantly different from normal distributions of unspecified mean and variance. If normality was established, we applied a *t*-test to compare the means of two populations or an ANOVA test if comparisons were made between more than two populations. If normality was not established, the Wilcoxon rank-sum or Kruskal–Wallis tests were used, as non-parametric equivalents of the *t*- and ANOVA tests, respectively. To calculate the significance of differences in categorical properties, we applied a χ^2 test. Relationship between groups was assessed with the non-parametric Spearman's rank correlation test. The significant level used for all of the tests was $P < 0.05$. Unless otherwise specified, population measurements were presented as the arithmetic mean ± SEM.

Results

General observations

A total of 107 visually responsive neurones were studied in 53 vertical electrode penetrations through the visual wulst of five owls. Typically, the restrained owls remained quiet for reasonably long periods of time, which facilitated the obtention of stable recordings. Only six isolated units were lost in the course of stimulation protocols. Offline spike-sorting analysis showed that these cells had merged into unsortable clusters. This left us with 101 neurones for the analyses detailed in the sections to follow. Another fact attesting to the stability of our recordings is that many single units could be held and characterized for as much as 3 h. As our recordings were limited to a few hours, we could only obtain a small yield of neurones per track (approximately two), even though we occasionally isolated as many as five units in a single penetration.

The response properties of the cells that we encountered were consistent with those previously described in other owl species (Pettigrew & Konishi, 1976; Pettigrew, 1979). Visual receptive fields were usually well defined and small; they never exceeded 5° in their largest dimension. Almost all cells in our sample were responsive to stimulation of either eye (Fig. 1A). Only three cells were found to be exclusively driven by one eye (Fig. 1B). At this point, it is important to reiterate that the grating and plaid stimuli that we subsequently used to characterize the directional responses of neurones were only presented to the dominant eye. Cells in our sample also typically showed tuned profiles for the spatial and temporal frequency of optimally moving full-contrast gratings. In some cases, we determined quantitatively the preferred value for these two dimensions and found them to be consistent with our qualitative estimates (Fig. 1C and D). Pettigrew (1979) reported the presence of several cell classes in the owl visual wulst, most of them having their correspondent in the mammalian V1. The response profiles that we encountered were consistent with many of these classes. Most notably, this also includes a cell type known as 'black bar specialists', unique for their preference to orientated dark bars moving against a light background.

To estimate the depth of our recordings within the visual wulst, we relied on readings from our microdrives, using as reference the electrode entrances into and exits from the neural tissue. Clearly, such estimates should be used with caution, as they are prone to inaccuracies due, for example, to tissue dimpling. However, the fact that readings made at the entrances usually coincided with those at the exits argues that the latter phenomenon was probably not a significant source of error. The distribution of our depth estimates ranged from 10 to 2360 μm. Most cells (∼ 80%) were recorded within the first 1200 μm, a depth that corresponds approximately to the lower border of the most superficial and thickest layer of the visual wulst (∼ 40% of the thickness of this structure), namely the hyperpallium apicale (HA), which is the main output layer (Karten *et al.*, 1973). The visual wulst extends further down for another 1600 μm (making up a total of approximately 2800 μm), where there are three additional layers (Karten *et al.*, 1973; Pettigrew, 1979; Reiner *et al.*, 2004): the interstitial nucleus of HA, hyperpallium intercalatum and hyperpallium densocellulare. According to our microdrive readings, only a few cells (∼ 20%) were sampled from within the interstitial nucleus of HA (granular layer) and none from the hyperpallium intercalatum or hyperpallium densocellulare.

Direction-selective response properties

To test whether visual wulst neurones are capable of signalling global motion, we restricted the analyses to neurones that exhibited at least some degree of directional selectivity. An objective assessment of this property was based on the evaluation of neuronal responses to the sinusoidal gratings used in the plaid protocols. Such gratings had optimal, or close to optimal, spatial and temporal frequencies, and their Michelson contrast was 0.45. Three out of the 101 well-isolated units were excluded because their mean firing rates across all stimulus directions did not significantly exceed baseline levels. Although these neurones had well-defined visual receptive fields, their activity was in fact suppressed in the presence of moving gratings. Another group of nine neurones was also excluded from our sample because they were judged to be omnidirectional after ANOVA performed across the 16 different directions of stimulus drift (see Materials and methods). Of the remaining 89 neurones, 67 (around 75%) were classified as directional selective, as their DI values were equal to or greater than the cut-off value of 0.5 (see Materials and methods). The remaining 22 cells were classified as non-direction selective.

The pattern of directional responses during presentation of gratings is shown for two representative neurones in Fig. 2A and C. It can be observed in this figure that both neurones responded selectively to particular directions of motion, exhibiting sustained discharge rates throughout stimulus presentation after occasional initial transient components. These transient components were not considered for the main part of our analysis (the first 200 ms after stimulus onset was

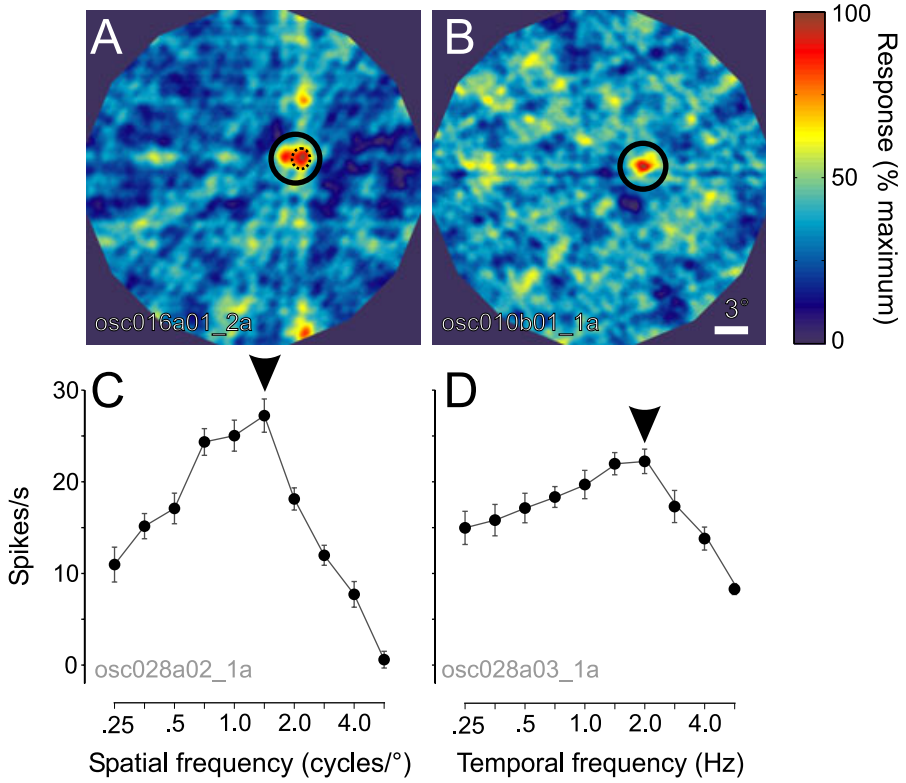

FIG. 1. Representative examples of receptive field properties in the visual wulst of the awake burrowing owl. Top panels show results of a quantitative receptive field-mapping procedure applied to (A) a binocular cell (the type of cell most frequently encountered in our experiments) and (B) a monocular cell, driven by the contralateral eye (a type of cell rarely found). The mapping procedure consisted of constructing two-dimensional maps of neuronal responses to a binocularly presented single bar (10° in length and 0.5° in width) swept across the screen in 16 different orientations with 10 repetitions of each. The maps were normalized to the maximum amplitude of the responses. The centre of the receptive field was defined as the point in the two-dimensional map of maximal responsiveness indicated by the solid-line circle. In the case of the binocular unit shown in A, two distinct but partially overlapping patches of more intense activity can be seen, indicating the presence of two receptive fields, one for each eye. Stimuli subsequently used in the main experimental protocols were always monocularly presented in the centre of the receptive field of the dominant eye, i.e. the eye for which greater responses were obtained (dotted-line circle). (C) Spatial-frequency tuning curve of a cell, measured with a full-contrast grating drifting in the preferred direction at a rate of 1 Hz. (D) Temporal tuning curve of the same cell shown in C, measured with the same grating at a fixed spatial frequency of 2 cycles/°. In both tuning curves, data points represent the mean spike rate (spikes/s) for 10 repetitions of 2 s stimulus presentations minus spontaneous activity. Error bars indicate ± SEM. The arrows indicate the optimal frequency values.

excluded), as they could have been induced by stimulus features unrelated to motion.

Directional tuning curves of the neurones whose responses are represented in Fig. 2A and C are plotted on a linear scale in Fig. 2B and D, respectively. We also show the fits that we applied to the tuning curves in order to estimate the directional tuning half-widths at half-maximum response. As apparent in both examples, and true for the rest of our sample, the fits provided a good description of the data. Only six out of 89 neurones had to be discarded for not having passed our goodness-of-fit criterion (R^2, see Materials and methods). For the remaining 83 neurones, R^2 was on average 0.91 (± 0.09 SD; range 0.81–0.99). In other words, 91% of the data could be explained by the fits. The latter were based on the sum of two von Mises functions, whose parameters for peak positions, heights and widths were free. Such parameters could be adjusted to obtain adequate descriptions of the unimodal tuning profiles of strongly directional cells (DI value around 1, Fig. 2B), as well as the bimodal profiles of directional cells less strongly selective due to subsidiary peaks in the antipreferred direction (Fig. 2D). As a consequence of this, the higher peak of the fits, from which our estimates of bandwidths were derived, was always found around the preferred direction.

Population data of DIs and tuning bandwidths are presented as histograms in Fig. 2E and F, respectively. The strength of directional selectivity ranged from non-directional (DI = 0.10) to strongly unidirectional, with suppression in relation to spontaneous activity in the antipreferred direction (DI = 1.35). For the large subpopulation of direction-selective cells, DI values were concentrated around a mean of 0.9, indicating a tendency towards unidirectionality without inhibition in the antipreferred direction, which was seen only in 20% of cells. The variability of tuning bandwidth values, which was apparent in the tuning curves shown in Fig. 2B and D, was reflected in the broad distribution shown in Fig. 2F (range 14.2–61.0°). The mean for the whole sample was 28.0° and roughly 45% of the cells had bandwidth values ranging between 20 and 30°. Values for directionally selective cells were not significantly different from those of non-direction-selective cells (27.8 ± 1.25° vs. 29.0 ± 3.0°, respectively; Wilcoxon rank sum test, $P = 0.89$).

Among the population of directionally selective neurones, no preferred direction was represented significantly more often than would be expected of a homogeneous distribution ($\chi^2 = 22.1$; DoF = 15; $P = 0.105$). However, we did observe a certain bias for downward motions. Preferred directions of 270° were indeed seen twice as often as any of the other 15 angular values. Interestingly, a similar bias is apparent in the middle temporal (MT) area of the primate (Albright, 1984, 1989) and has been found to be significant in a study by Diogo *et al.* (2003).

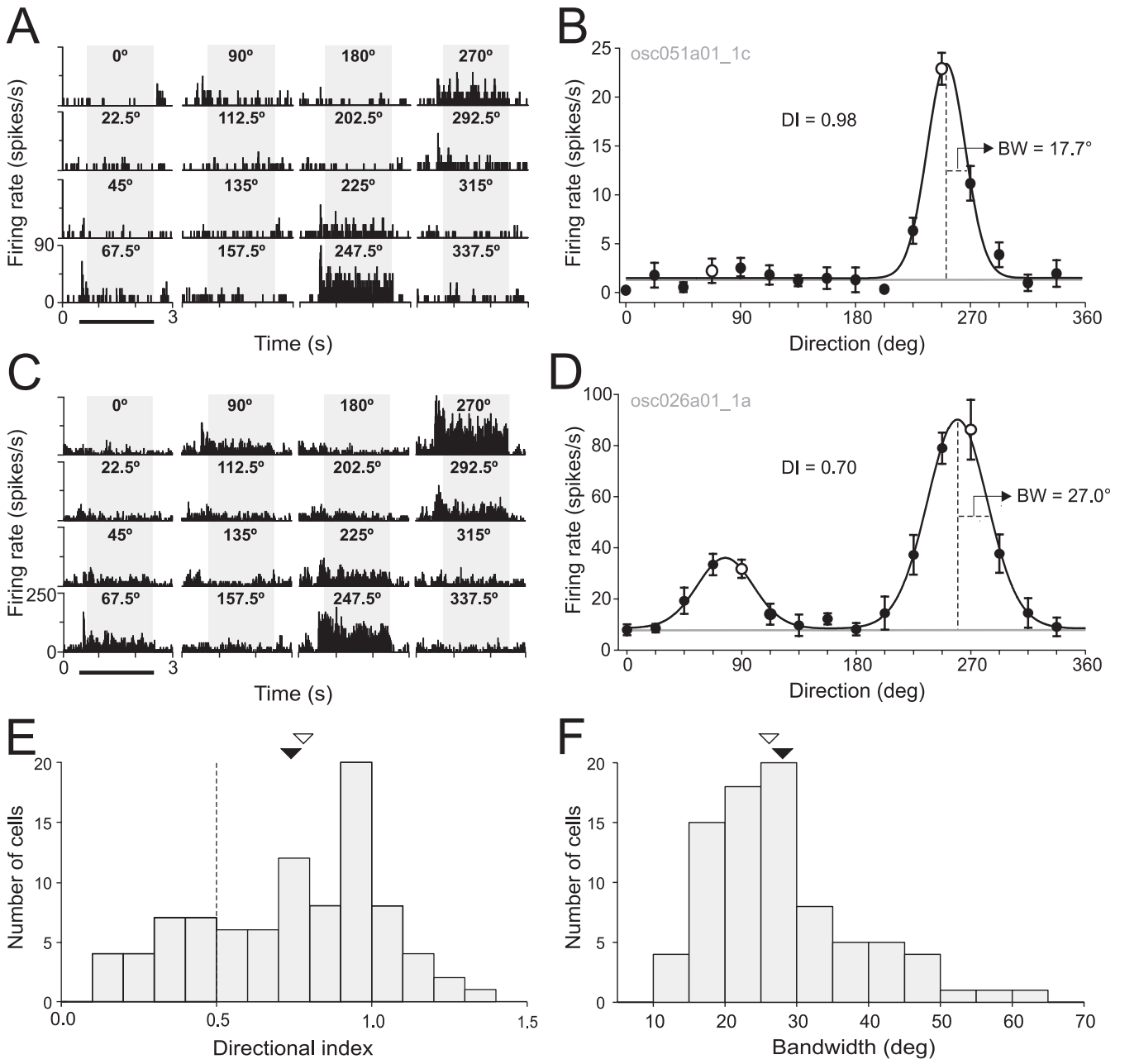

FIG. 2. Directional tuning properties of 89 neurones sampled in the visual wulst. (A–D) Responses of two representative direction-selective neurones to 45% contrast sinusoidal gratings drifting at optimal spatial and temporal frequencies. Left panels: Responses are shown as average peristimulus time histograms (PSTHs) for 16 different stimulus directions (as indicated on top of each histogram) with 10 repeated measures at each using a randomized order of stimulus presentation (bin size = 10 ms). Spontaneous activity was collected before the onset of the stimulus (first 500 ms of the PSTHs). Gratings were presented from 500 to 2500 ms, as indicated by the bars beneath the first column of PSTHs. The grey-shaded rectangles delineate the 1800 ms period considered for the analyses, after the exclusion of the 200 ms period following stimulus onset. Right panels: Direction tuning curves in which mean firing rate (spikes/s), computed over the whole stimulation period minus the initial 200 ms, is plotted as a function of stimulus direction. The open circles indicate mean response amplitude in the preferred and antipreferred direction. Solid lines represent the fitted models used to determine the half width at half height of the model peak response, which was our measure of the cell's directional tuning bandwidth (BW). Bars indicate the confidence interval of the mean at the 95% level. The models were based on the sum of two von Mises functions, as described in Materials and methods. The grey horizontal line indicates the level of spontaneous activity. (E) Distribution of direction indices (DIs). The DI has positive values that increase from 0 to 1 as mean response in the preferred direction increase relative to that in the antipreferred direction, with values above 1 if the response is inhibited (below spontaneous activity level). The dashed line indicates the boundary between orientation-selective (DI < 0.5) and direction-selective (DI ≥ 0.5) neurones. (F) Distribution of direction bandwidths. Mean and median values are represented for both DI and bandwidth distributions by the filled and empty triangles, respectively.

Neuronal responses to plaids

The 67 direction-selective units were tested with respect to their ability to signal the global motion of plaid patterns. The key aspect of the test was the dissociation of component and pattern motions in the plaid stimulus, as the apparent motion of the whole plaid was intermediate to the actual motion of its component gratings. If a neurone is selectively responsive to global pattern

motion, its tuning curves for the grating and plaid stimuli should be essentially the same. However, if a neurone is selectively responsive to component motion, its tuning curve for the plaid stimulus should be bilobed, peaking when either of the component gratings matches the preferred direction of motion of the neurone.

A representative sample of three CDS cells is shown in Fig. 3. In this and in the next figure, responses are plotted in a polar representation where the distance of a point from the origin represents the firing rate in spikes per second and the angle indicates the direction of motion of the stimuli. In response to gratings drifting in 16 different directions through its receptive field, the first neurone (Fig. 3A) had a marked preference for the upward direction and the strength (DI = 0.91) and narrowness of the bandwidth (BW = 27.0°) of its directional tuning were typical of many direction-selective neurones in our data set (see Fig. 2A and B). In response to plaids (Fig. 3B), this neurone showed two peaks of activity at motion directions symmetrically opposite to one another by an angle of 45° with respect to the upward direction. This is what would be expected from a neurone that responds independently to each of the component gratings of 90° plaids. To verify this observation objectively, we used the direction tuning measured for gratings to predict the model responses of an ideal CDS cell (represented by the dotted black lines in Fig. 3B, D and F) and of an ideal PDS cell (not shown) to plaids, and compared those models with the experimentally measured plaid tuning curves. The predicted direction tuning for a CDS model neurone is the sum of the direction tunings for the two gratings presented alone, whereas the prediction for a PDS model cell is identical to the measured direction tuning for gratings (see *Data analysis* section in Materials and methods). It can be observed that the plaid tuning curve of the unit in Fig. 3B closely matches the CDS prediction. This was confirmed numerically by computing the partial correlation coefficients between the plaid responses and the two model predictions. With a high component partial correlation ($R_c = 0.95$) and low pattern partial correlation ($R_p = -0.15$) this unit was unambiguously classified as CDS. A similar classification was obtained for cells that exhibited a variety of directional properties, such as, for example, a lower DI (Fig. 3C and D) or a broader tuning bandwidth (Fig. 3E and F).

Although most of the direction-selective neurones that we sampled within the visual wulst showed a CDS profile to drifting plaids, several of them did not concur with either component or pattern prediction. Figure 4 exemplifies three different reasons why this occurred. The unit in Fig. 4A and B illustrates the case of several neurones broadly tuned for gratings that were unclassifiable because their responses to plaids, although clearly directional, were somehow intermediate between the component and pattern predictions. The example in Fig. 4C and D illustrates another type of unclassified cell that had an attenuated response to plaids, without any clear unidirectional or bidirectional response profile. The behaviour of the cell in Fig. 4E and F was rather atypical. This unit was highly directional (DI = 1.06) and broadly tuned (bandwidth, BW = 49.16) for the gratings. In response to plaids, it showed two clear peaks at angles corresponding to each of the components of the plaids. However, it failed to be classified as CDS because its plaid tuning curve was rotated anticlockwise by an angle of around 45° with respect to the component prediction. This angular shift seemed to be genuine as it was found again when we repeated the experiment with 135° plaids (see below and Fig. 7). Notably, when we artificially compensated for this angular deviation by rotating the actual plaid tuning curve by a 45° clockwise angle, the cell became CDS with $R_c = 0.60$ and $R_p = -0.23$.

Figure 5 shows a scatter plot in which the values of the pattern and component correlation coefficients of all direction-selective visual wulst neurones are plotted against one another, as first used by Movshon *et al.* (1985). The plot is divided into three statistically distinct regions that were used to categorize neurones as CDS, PDS or unclassifiable (regions labelled as COMPONENT, PATTERN or UNCLASSIFIED, respectively). The predominance of CDS cells in our population data is evident. Out of 67 cells, 54 (~80%) were indeed classified as such. They responded best to a moving plaid pattern when the axis of motion of one of the component gratings coincided with their preferred axis of motion and their tuning curves were best described by the component prediction. The remaining 13 cells (~20%) were unclassifiable and no PDS neurones were encountered. Globally, the proportions of CDS and unclassifiable cells found in this study are fairly similar to those reported in the striate cortex of cats and primates (Movshon *et al.*, 1985; Gizzi *et al.*, 1990; Guo *et al.*, 2004). However, in the awake owl, we did not find the small population of PDS cells (9%) that Guo *et al.* (2004) encountered in V1 of monkeys performing a fixation task.

In order to assess the degree to which a cell expressed component-type selectivity more strongly than pattern-type selectivity, we computed a component index by subtracting the variance accounted for by the component prediction from that accounted for by the pattern prediction ($R_c^2 - R_p^2$). Positive values signify close conformity with the component prediction, whereas negative values support the pattern prediction. The distribution of these values is shown in Fig. 6A. As expected, the difference between the mean component indices of CDS cells (0.62 ± 0.02) and those of unclassifiable cells (0.10 ± 0.05) was highly significant (Wilcoxon rank sum test, $z = -5.3$, $P < 0.001$). The large majority (85%) of CDS cells had a component index greater than 0.5, indicating that most neurones classified as CDS by our statistical procedure retained a low degree of pattern motion selectivity. Moreover, it is interesting to note that the degree of component selectivity of a neurone within the visual wulst could not be predicted from its directional selective properties measured with drifting gratings only. As is apparent in Fig. 6B, there was no significant relationship between component motion selectivity and the strength of a neurone's direction selectivity (Spearman rank correlation, $\rho = -0.04$, $P = 0.61$). There was also no significant systematic shift to component motion selectivity with increasing direction tuning width (Spearman rank correlation, $\rho = -0.16$, $P = 0.88$, Fig. 6C).

Effect of plaid angles on partial correlation coefficients

The reliability of partial correlation coefficient measurements depends, to some extent, on choosing an appropriate plaid angle. For example, it is obvious that the bilobed profile in the plaid tuning curve of a typical CDS cell would not show up for plaid angles that are much smaller than the direction tuning width of the cell. In general, it is also true that the smaller the angle between the two component gratings of the plaid, the more similar the component and pattern predictions will tend to be, and consequently the less likely are the chances of finding a definitive difference between the two predictions. Ultimately, this situation will increase the likelihood of categorizing cells as unclassified and, at this point, it is important to stress that cells categorized as such are not somehow 'intermediate' between CDS and PDS cells. Rather, they should be considered as cells for which the particular test conditions and statistics used were not sufficiently sensitive to classify them. In the present study, we chose a plaid angle of 90°, a value that has often been used to probe the pattern motion selectivity of cells in the mammalian striate cortex (Movshon *et al.*, 1985; Gizzi *et al.*,

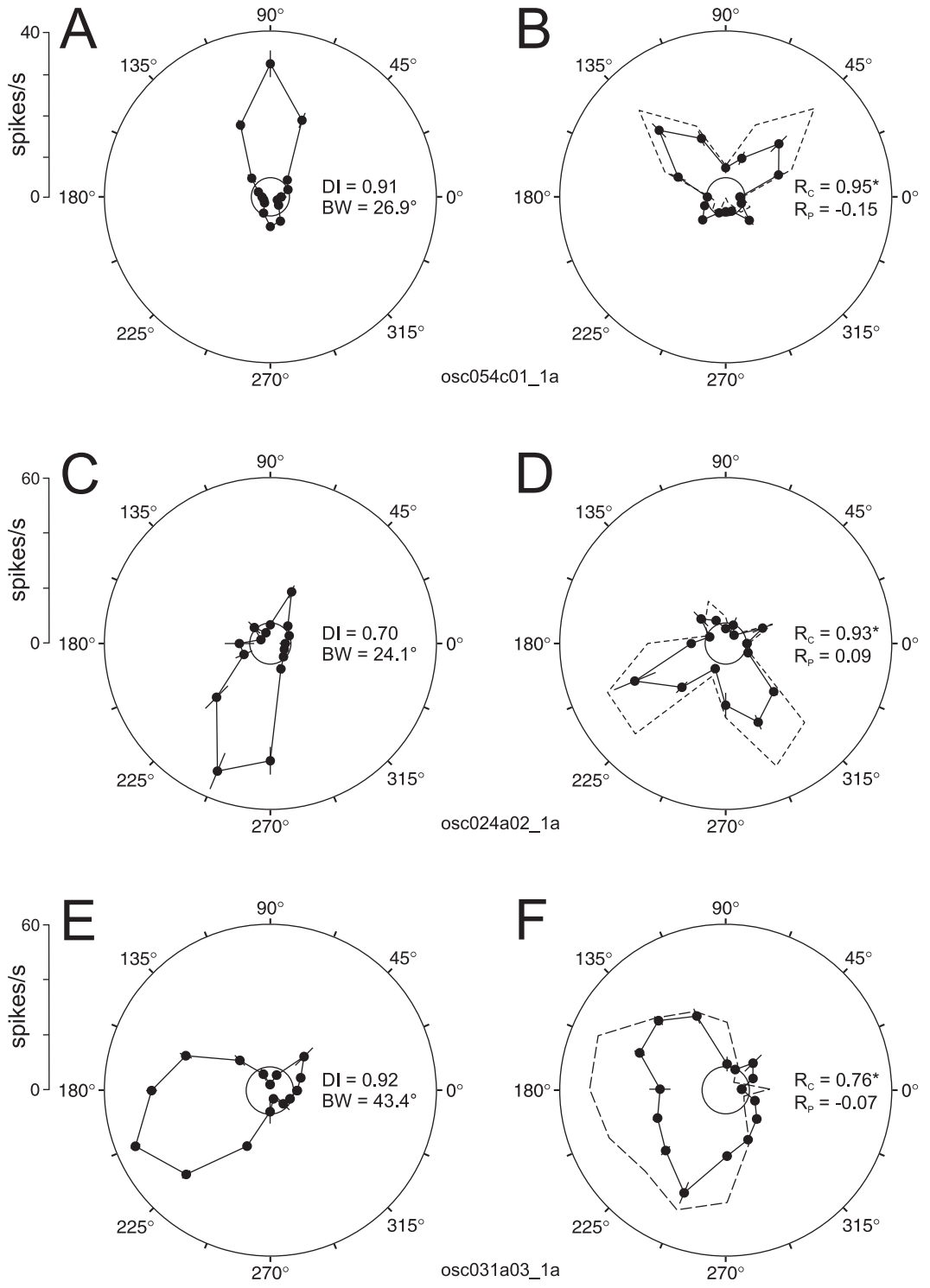

FIG. 3. Directional tuning of three component direction-selective neurones to drifting sine wave gratings (A, C and E) and 90° plaids (B, D and F). The angle on each polar plot shows the stimulus direction of motion, whereas the radial dimension represents response amplitude (spikes/s). The black circle centred on the origin indicates the mean level of spontaneous activity. The solid lines and data points depict the actual response of the neurone, and error bars represent 1 ± SEM. The dashed lines in B and D indicate the component prediction, which represents the direction tuning for plaids if the neurone responded only to the motions of the two component gratings. This component prediction is generated by adding two direction tuning curves obtained for gratings, with one rotated 45° clockwise and the other rotated 45° anticlockwise. DI, direction index; BW, directional tuning bandwidth defined as in Fig. 2. R_c and R_p are the partial correlations for the component and pattern predictions, respectively. The asterisk indicates statistical significance ($P \leq 0.1$).

1990; Tinsley *et al.*, 2003; Guo *et al.*, 2004). Given the distribution of direction tuning bandwidths and the relatively small proportion of unclassifiable cells described earlier, we believe that this choice was suitable for capturing the motion sensitivity of visual wulst neurones in response to plaid patterns. Even so, we assessed the likelihood of this inference by repeating our partial correlation measurements with 135° plaids for a subset of neurones. It is clear from the graph in Fig. 7 that a substantial 45° increase in plaid angle did not fundamentally

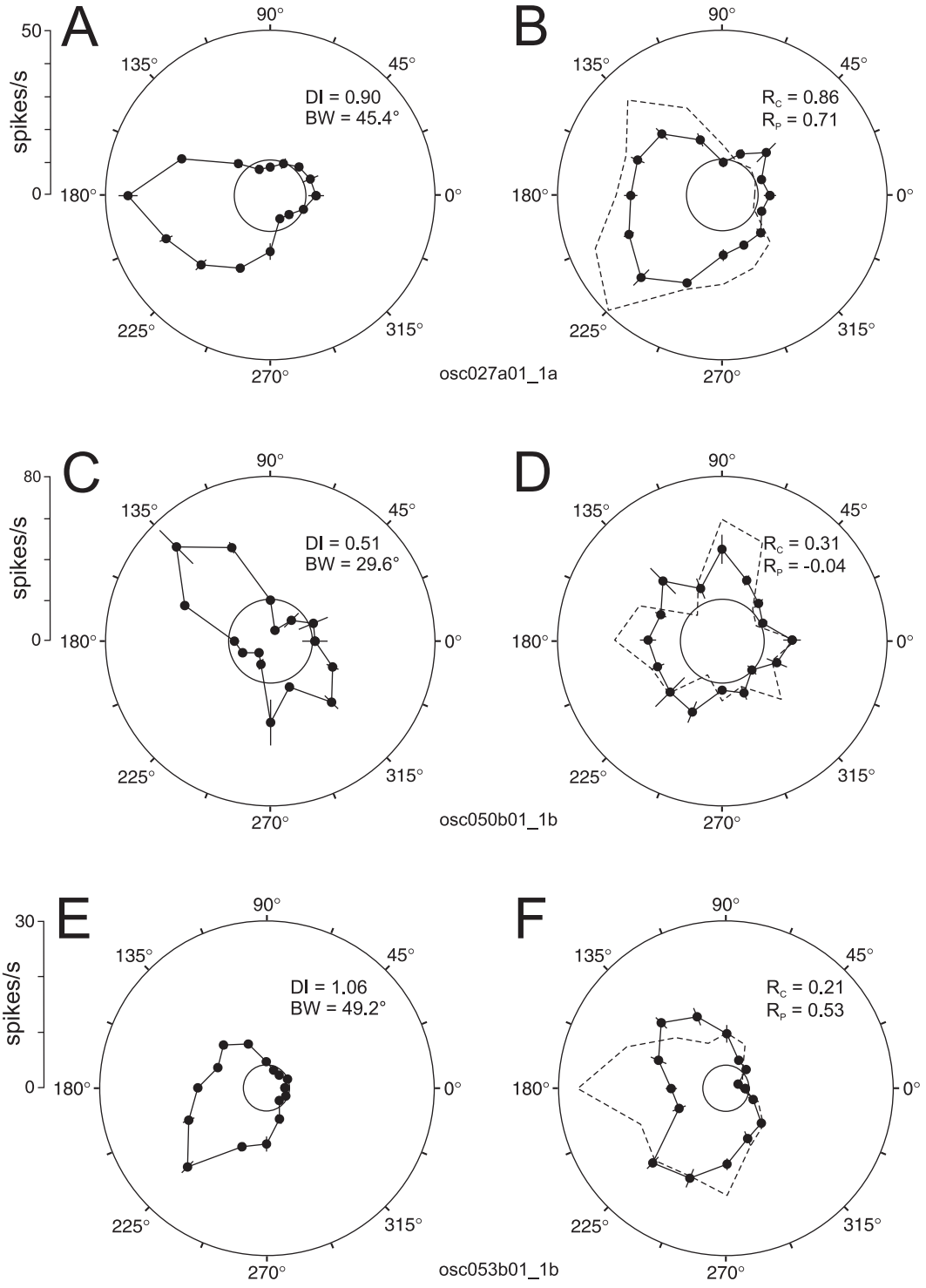

FIG. 4. Directional tuning of three unclassified neurones to drifting sine wave gratings (A, C and E) and 90° plaids (B, D and F). Conventions as in Fig. 3. Note that none of the partial correlation values are marked with an asterisk because for unclassified neurones such values do not reach statistical significance.

change the classification of the 17 retested neurones. Only one of them changed category, migrating from the UNCLASSIFIED to the COMPONENT zone. Across the whole cell sample presented in Fig. 7, changes in correlation coefficient values could be observed following a plaid angle increase. However, as determined by the Wilcoxon signed-rank test, R_c values calculated for 90° plaids were not significantly different from those calculated for 135° plaids ($z = -1.21$, $P = 0.23$). This was also true with respect to R_p ($z = -1.30$, $P = 0.20$) and component index ($z = 1.10$, $P = 0.27$) values.

Response inhibition to plaid patterns

The partial correlation method that we used to classify neurones into CDS and PDS effectively compares the shape between the tuning

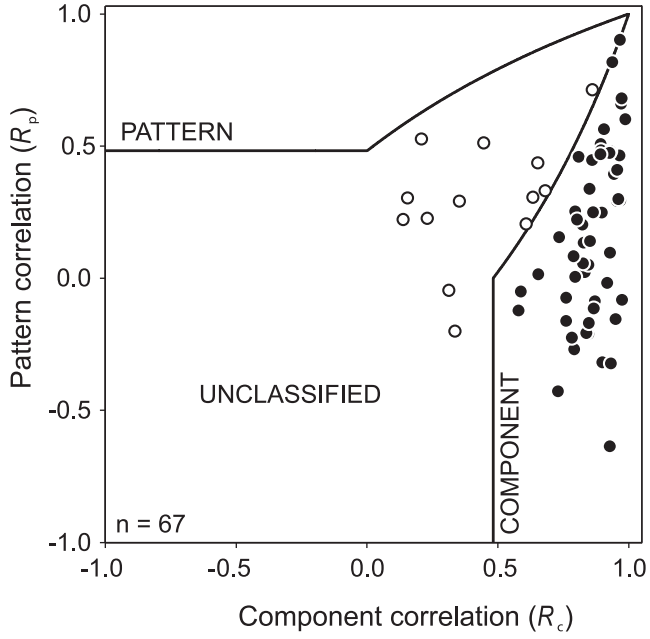

FIG. 5. Scatter plot of partial correlations for the component prediction (R_c) and pattern prediction (R_p) of 67 direction-selective neurones sampled within the owl visual wulst. The graph shows partial correlations in response to 90° plaids. The bullet-shaped line divides the plot into three zones of interest. Points falling in the region marked COMPONENT indicate cells whose R_c significantly exceeds either zero or the value of R_p. Such cells are classified as component direction selective (CDS). Similarly, data points belonging to the region marked PATTERN contain those cells for which R_p significantly exceeds either zero or the value of R_c. Such cells are classified as pattern direction selective (PDS). The intermediate region referred to as UNCLASSIFIED contains cells for which neither correlation coefficient differed from zero or the two coefficients did not differ significantly from each other. Cells classified as CDS are indicated as black filled circles, whereas those unclassified by the partial correlation method are indicated as open circles. Note that no cell satisfies the requirements for PDS classification. The statistical procedure used to define the three regions of interest in the scatterplot is based on a critical value of t for 10% level of significance (for more details see *Data analysis* section in Materials and methods).

curves measured for plaids and the predicted tuning curves for component and pattern direction selectivity. However, this comparison does not take into account absolute differences in response strength. This is an important point, considering the fact that response levels to plaids were often lower than those predicted from the gratings (see, for examples, Fig. 3B and D). In order to quantify the relative magnitude of these inhibitory effects in our dataset, we calculated a plaid inhibition ratio, which compares the actual peak response to plaids with the predicted peak response. As apparent in Fig. 8, the values of this ratio were normally distributed and tightly clustered around a mean of 0.72 ± 0.08. Only seven cells (10%) showed a plaid peak response higher than the maximal response of the model prediction (plaid inhibition ratio > 1). No statistical differences were found between the distributions of CDS and unclassifiable cells. Strikingly similar mean ratios have been reported in other plaid studies carried out within the mammalian V1 (Movshon *et al.*, 1985; Gizzi *et al.*, 1990; Guo *et al.*, 2004). In those studies, the suppression effect of plaids is interpreted as a manifestation of a form of inhibition known to exist in the striate cortex, namely cross-orientation inhibition (Blakemore & Tobin, 1972; Morrone *et al.*, 1982; Bonds, 1989; DeAngelis *et al.*, 1992). Accordingly, the response to one of the plaid component gratings would be inhibited by the presence of the other component.

Temporal dynamics of component direction selectivity

All of the observations made so far were based on analyses in which neuronal discharges occurring within the first 200 ms of stimulation were excluded. By doing so, we sought to minimize the potential contamination of activity not directly related to the motion direction of the stimuli. However, as exemplified in Fig. 2A and C, the presence of transient peaks of activity shortly after stimulus onset was mostly noticeable for stimuli moving at or near preferred and/or antipreferred directions, suggesting that these early responses are, at least to some extent, directionally selective. We therefore decided to examine the component/pattern motion selectivity of our sample during this initial 200 ms period, comparing it with that determined for the latter (more sustained) part of the response.

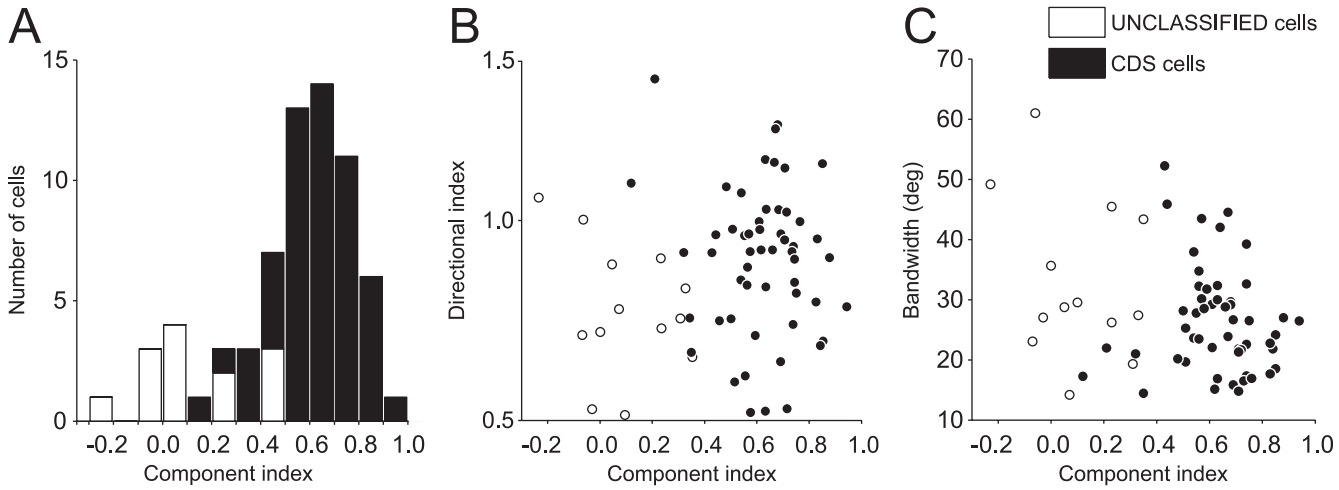

FIG. 6. Relationship between component motion selectivity and direction selectivity for the population of directionally selective neurones. (A) Distribution of component index values calculated for each of the 67 direction-selective visual wulst neurones in response to 90° plaid patterns. The component index is equal to $R_c^2 - R_p^2$ and reflects the strength of component selectivity relative to pattern selectivity. (B) Scatter plot of component vs. direction indices. (C) Scatter plot of component indices vs. directional tuning bandwidth values for the same population of neurones. Black filled symbols refer to component direction-selective (CDS) neurones and open symbols indicate unclassified neurones. R_c, partial correlation coefficient for the component prediction; R_p, partial correlation coefficient for the pattern prediction.

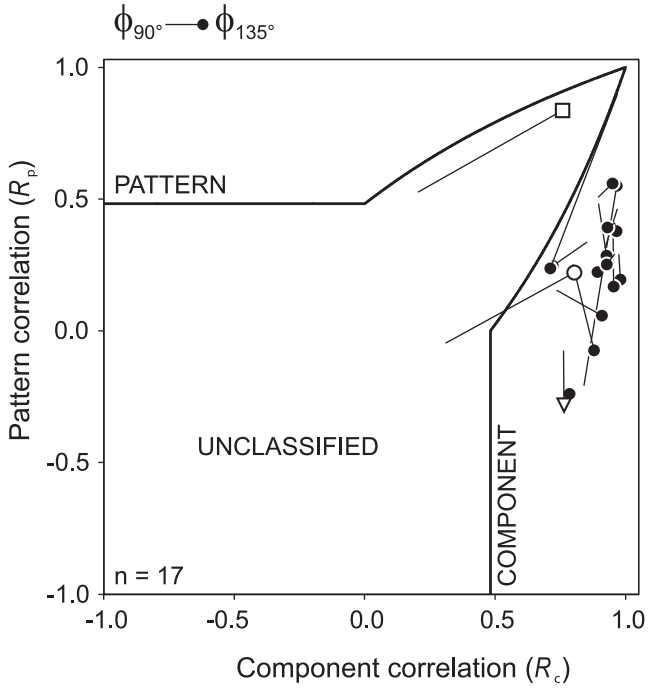

FIG. 7. Influence of plaid angle on the partial correlations for component prediction (R_c) and pattern prediction (R_p) of 17 direction-selective neurones. For each cell, a line connects the partial correlations in response to 90° plaids (no symbols) to those obtained with 135° plaids (symbols). The direction of the lines therefore illustrates the shift in the partial correlations due to the change of plaid angle. All black circles refer to cells that have not been presented in previous figures. Other units: open triangles, osc031a03_1a; open squares, osc053b01_1b; and open circles, osc050b01_1b. The tuning curve of these units has been presented for 90° plaids in Figs 3 and 4.

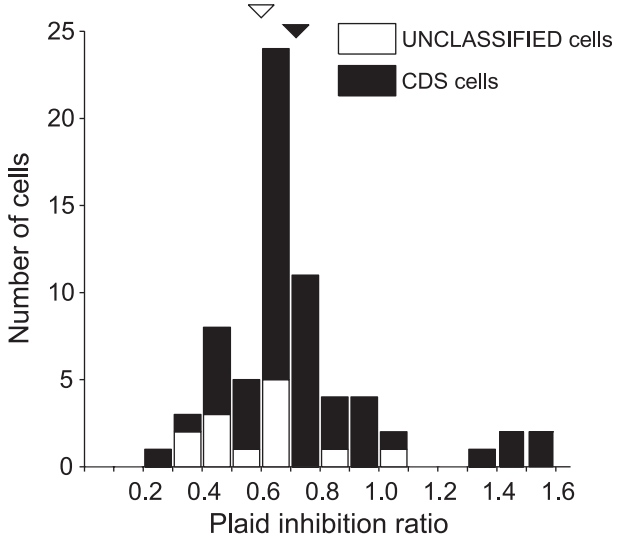

FIG. 8. Distribution of plaid inhibition ratios for direction-selective neurones ($n = 67$). A ratio was calculated for each cell by dividing the actual peak response to plaids by the peak response predicted from the model of component direction selectivity (with spontaneous activity subtracted). A ratio < 1 indicates plaid inhibition and a ratio > 1 indicates facilitation. Note that the majority of cells show some sign of inhibition. Black filled bars refer to component direction-selective (CDS) neurones and open bars indicate unclassified neurones. Mean values for each cell category are represented by the triangles that are colour coded to conform to the convention used for the bars.

Figure 9 presents the distribution of partial correlation coefficients in four cumulative windows starting from 0 to 50 ms after stimulus onset and expanding by 50 ms in each successive analysis window. The temporal evolution of these coefficients is shown for five representative cells (Fig. 9A) and for the whole population of direction-selective neurones (Fig. 9B). The colour assignment of the data points in these plots refers to the cell classification established in Fig. 5, thereby providing a means of comparing this previous classification with that obtained for the first 200 ms of stimulation. Two features stand out from this figure. The first concerns the population of unclassified cells, which maintain themselves steady in the UNCLASSIFIED region from as early as the first 50 ms window except for one cell, which expresses significant, albeit less stable, PDS tuning. The second concerns the population of CDS neurones, which migrates gradually from the UNCLASSIFIED to the COMPONENT region of the plot as the window is enlarged to 200 ms. In the first 50 ms, only one out of 54 cells (2%) is classified as CDS. This proportion grows steadily to 11/54 (20%), 24/54 (44%) and 36/54 (67%) over the second, third and fourth plots, respectively, indicating a significant early development of CDS-like tuning. However, by 200 ms of stimulus presentation, one-third of CDS neurones have not significantly gained their characteristic response tuning, as determined when averaging the later part of the response. One possible explanation for this is that stimulus features other than motion may be interfering with responses right after stimulus onset. Nevertheless, care is needed in interpreting this result as such, because responses are being averaged across two windows with very different time spans. Averaging spike counts over shorter intervals may result in noisier tuning curves, favouring unclassifiable outcomes of directional selectivity.

The above results and considerations enticed us to examine, using a different approach, the way in which component selectivity varied during the time course of the entire stimulus presentation. For this, we calculated the average component index for each of a series of 100 ms windows sliding over the whole period of stimulus presentation in 50 ms increments. Results from this analysis are presented in Fig. 10A. Despite a fair amount of variability among cells, it is clear that the strength of component selectivity dynamically unfolds as an initial transient followed by a relatively steady component that remains well above the level observed at stimulus onset and offset. A sharp increase is already noticeable during the first 100 ms response window after stimulus onset (second data point of the curve) and peaks during the fourth window centred at 150 ms. This result suggests that the computation of component selectivity is a process that builds up during the first 150 ms of the neurones' response, confirming the results presented in Fig. 9. Furthermore, it shows that, although higher during the early phase of the response, the strength of component selectivity settles to a sustained level throughout the response to stimulus motion. As can be seen in Fig. 10B, the firing rate of the CDS neurone population in response to both gratings and plaids shows a fairly similar temporal profile, indicating that the strength of component selectivity is somehow linked to changes in neuronal responsiveness.

Discussion

The present experiments were performed with the aim of obtaining more information about the directional selectivity of neurones in the visual wulst of the owl. Responses to sinusoidal gratings were analysed to characterize direction-selective neurones in terms of their overall proportion, directional strength and tuning precision. Although

partially available for the wulst of pigeons (Miceli *et al.*, 1979) and chicks (Wilson, 1980b), such a quantitative description had not been explicitly reported for the owl. In our study, responses to gratings were also compared with those to plaids in order to evaluate whether wulst neurones are capable of spatially integrating local features for signalling the global motion of a complex stimulus. Despite its fundamental importance for understanding motion perception, this question has never been addressed in the visual wulst. In the owl, this area is far more developed than in most other birds and has been shown to contain neurones that respond to illusory contours, which

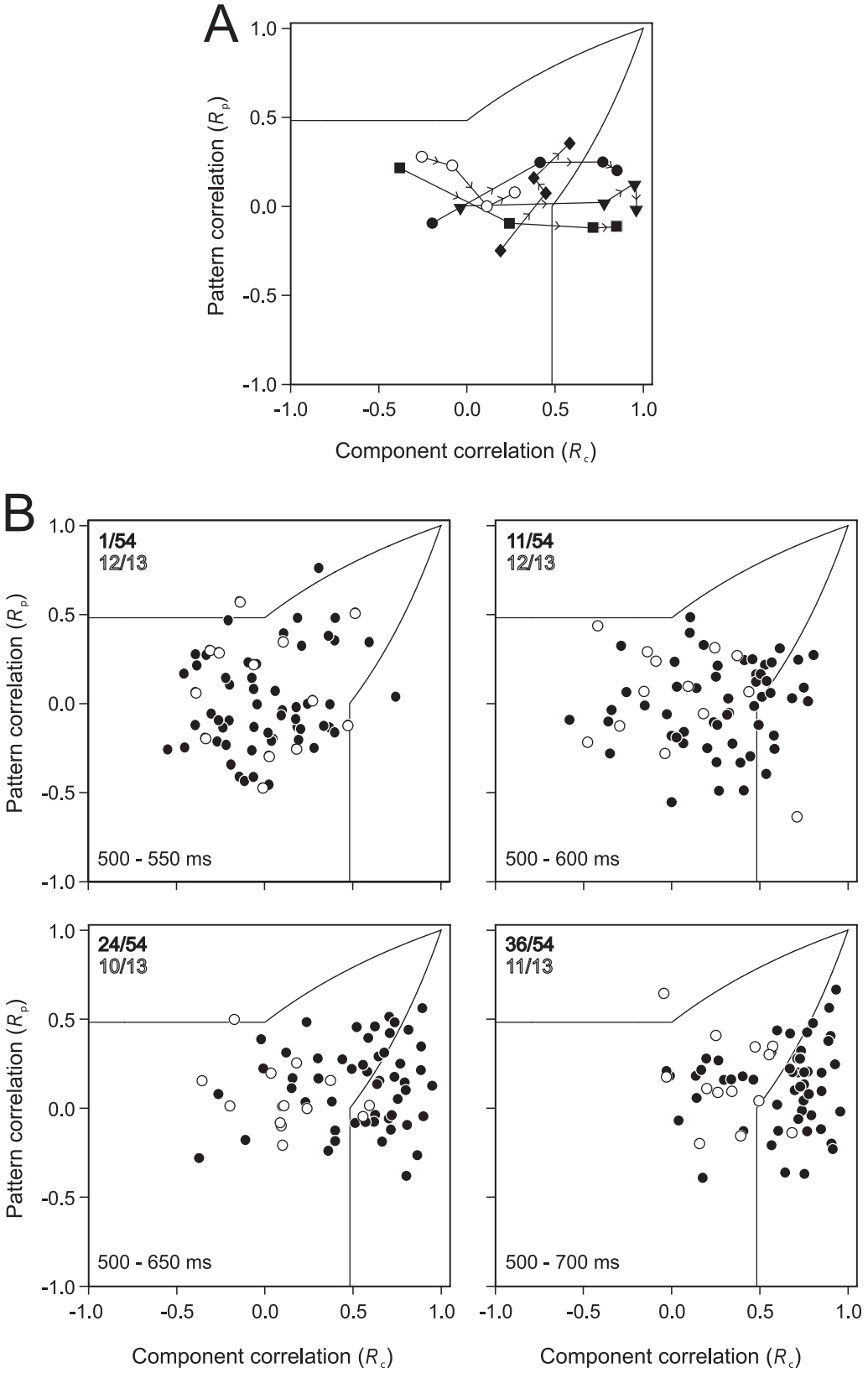

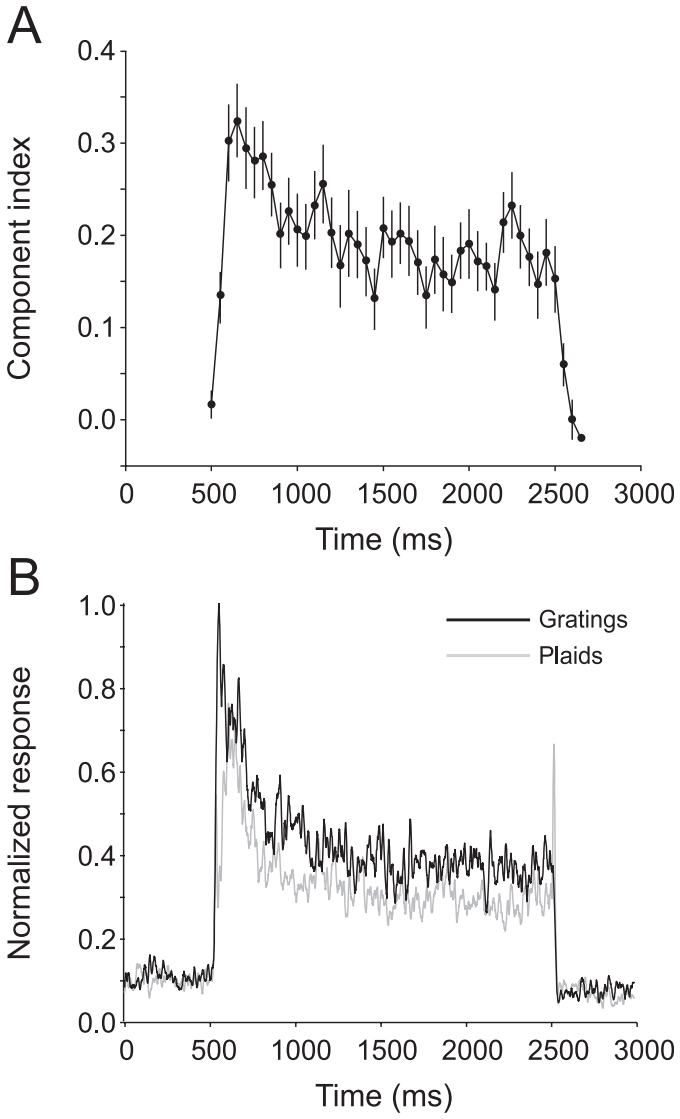

FIG. 10. Population summary of the temporal evolution of component direction-selective (CDS) neurone responses. (A) Temporal dynamics of component selectivity during the whole period of stimulus presentation (from 500 to 2500 ms). Data points indicate the mean component index (± SEM) for the population of 54 CDS neurones calculated in 100 ms windows moving in 50 ms steps over time (sliding windows). (B) Population response to gratings (black line) and plaids (grey line) as a function of time for the 54 CDS neurones. For each cell, an average spike density function was generated by convolving the trial-averaged, 1-ms binned, peak response to a particular stimulus type (gratings or plaids). The convolution kernel was a Gaussian with a 15 ms SD. Spike density functions were then normalized by the population peak response to gratings and averaged across neurones. Note the relative inhibition of neuronal responses to plaids.

suggests that large-scale integration may take place within the wulst (Nieder & Wagner, 1999; but see Niu *et al.*, 2006). Here, we examined whether such global computation also takes place in the motion domain, as known to be the case in the mammalian visual cortex (Albright & Stoner, 1995).

Our findings can be summarized into two major points. First, the visual wulst of the owl contains a sizeable population of direction-selective neurones that respond robustly to one direction of an optimally orientated moving grating but little if at all to the opposite direction. On average, these neurones have relatively narrow directional tuning bandwidths, although a broad range of values can be observed. Second, when tested with plaids, direction-selective neurones do not show selectivity for the global motion of these stimuli. Instead, the majority yields bilobed tuning curves that can be well predicted by the linear sum of the responses to the two component gratings of the plaids measured separately. Thus, neurones usually show a CDS profile, responding to the motion direction orthogonal to the orientations of the contours that make up the plaid stimuli. The contribution of an orientation-sensitive mechanism in determining directional responses to plaids was further suggested by the fact that such responses were consistently lower than those to gratings alone and that this may be explained by the mutual inhibition of the two components in the orientation domain.

Altogether, our results indicate that directional selectivity is a distinctive characteristic of the visual wulst in the owl. They also indicate that the mechanisms responsible for directional responses are dependent on orientation-selective mechanisms sensitive to the motion of individual contours. Considering that wulst neurones usually have small receptive fields, the information that they are able to convey about object motion is therefore likely to be one-dimensional and local. In this respect, our study suggests that the motion aperture problem cannot be solved at the level of the wulst and leaves open the question as to how and where global motion is being recovered within the avian visual system. In order to ascertain the relevance of this issue, it would be necessary to demonstrate that owls are actually able to see the global motion pattern in plaids. However, there is no reason to believe otherwise, given the complex perceptual capabilities exhibited by these birds (see, for instance, Nieder & Wagner, 1999; van der Willigen *et al.*, 2003).

Receptive field properties in the visual wulst

Our findings confirm previous studies that report the presence of rather small receptive fields in the wulst. In the barn owl, Pettigrew (1979) found receptive fields as small as 1° in the region of central representation and even smaller receptive fields in the dorsolateral geniculate nucleus. The author also described a large over-representation of the central hemifield, with more than half of the total area of the wulst dedicated to the central 10°. Such visuotopic organization is typical of visual areas involved in fine-scale spatial analysis. *De facto*,

FIG. 9. Scatter plots of partial correlations for the component prediction (R_c) and pattern prediction (R_p) during the first 200 ms after stimulus onset. All neurones were subjected to the same analysis as that shown in Fig. 5, except that here spike count was performed in four cumulative time windows, starting at 500 ms (stimulus onset) and extending by 50 ms in each successive analysis window. (A) Representative examples of five cells (each indicated by a different symbol), where each point represents R_p and R_c values for a specific time window. To indicate the temporal evolution of partial correlation coefficients, successive analysis windows are linked by arrow lines. (B) Temporal evolution of R_p and R_c values for the whole population of direction-selective cells. The ranges of time windows are indicated at the bottom left of each plot. The bottom right plot shows the distribution of partial correlation coefficients computed in a response window that covers the entire 200 ms stimulus period excluded while preparing Fig. 5. Conventions are as in Fig. 5. In both A and B, the black-filled symbols represent the cells previously classified (in Fig. 5) as component direction selective and the open circles represent those cells that were not classifiable. In B, for each of these two categories (same colour code), the proportion of cells reaching the same classification as in Fig. 5 is indicated in the upper left corner of each plot.

a number of electrophysiological studies in the pigeon (De Britto *et al.*, 1975; Jassik-Gerschenfeld *et al.*, 1976) and the chick (Wilson, 1980a; Pateromichelakis, 1981), as well as more recent lesion studies in the pigeon (Hahmann & Güntürkün, 1993; Budzynski & Bingman, 2004), support the notion that this capacity for high-resolution spatial analysis is a relatively well-conserved trait of the avian thalamofugal pathway.

Our results are also relevant to another hallmark property of the visual wulst, namely the orientational selectivity of its neurones (Pettigrew & Konishi, 1976; Pettigrew, 1979; Wilson, 1980b). In the barn owl, 90% of the 579 cells studied by Pettigrew (1979) were orientation selective. According to the author, within the superficial layer of the wulst (HA), many orientation-selective cells also show a directional bias in their response to moving stimuli. As HA is the main output layer of the wulst (Karten *et al.*, 1973), and is where most of our recordings were made, our results consequently deal with the final stages of processing in the wulst. Here, we not only provide a more detailed quantitative description of directional responses but also present direct evidence that direction-selective cells are primarily orientation-selective inasmuch as they are only sensitive to the individual contours of plaids. In other words, direction selectivity in the wulst is always secondary to orientation selectivity, which reinforces the idea that this area is more specifically involved with the detailed analysis of object spatial configurations. It also suggests that more complex forms of motion analysis must occur, at least in part, in other areas of the avian brain.

Another clue to the importance of orientation selectivity in the wulst is that it appears to be organized into regular, columnar patterns. Neurones recorded in penetrations normal to the wulst surface were found to have closely similar orientation preferences, whereas in tangential penetrations the preferred orientation changed progressively and in small steps (Pettigrew, 1979). Using intrinsic signal optical imaging, Liu & Pettigrew (2003) recently confirmed the presence of these iso-orientation domains in the barn owl and further showed that such domains were comparable to those found in area V2 of cat and monkey cortex. Our finding of the suppressive effect of plaids on cell responses may provide a new element of information regarding the functional organization of orientation selectivity within the wulst. Indeed, as stated above, this result hints at the existence of cross-orientation inhibition, which implies that, in the wulst, regions of differing orientation preferences are interconnected by lateral inhibitory projections. In the mammalian V1, this type of circuitry has been associated with the sharpening of orientation tuning relative to that provided by thalamic afferents (Ferster, 2004). A modelling study has also shown that it may favour the emergence of directional selectivity (Wörgötter *et al.*, 1991). The above considerations should therefore prompt future work to investigate more thoroughly orientation-specific inhibition and its functional role in the wulst.

An important feature that sets owls apart from most other birds is the frontal placement of their eyes, which allows them to have a large degree of binocular overlap (Martin, 1984; Wylie *et al.*, 1994) and stereoscopic depth vision (van der Willigen *et al.*, 1998, 2002). It is presumed that the wulst plays an important role in mediating stereopsis in the owl, as it contains a large majority of neurones that are binocular and tuned to horizontal and vertical disparities (Pettigrew & Konishi, 1976; Pettigrew, 1979; Wagner & Frost, 1993, 1994; Nieder & Wagner, 2000, 2001a,b). The fact that all of the direction-selective neurones that we sampled ($n = 67$) were also binocular is interesting, as it raises the possibility that motion and stereoscopic signals get integrated and perhaps interact at the single cell level in the wulst. A number of psychophysical and physiological studies indicate that not only does such cue integration take place in the primate visual system but that it may also be of functional relevance (see, for example, Rogers & Collett, 1989; Bradley *et al.*, 1995; Bradshaw & Cumming, 1997). Theoretically, there are various advantages to processing motion and stereoscopic cues jointly (Richards, 1985). Foremost, both cues have the same prerequisite, which is to establish a correct match between retinal images. In the motion domain, this match needs to be established in time, across image sequences, whereas in the stereoscopic domain, the match needs to be made simultaneously between the eyes.

Incidence, strength and precision of directional selectivity

All of the functional properties previously reported for the visual wulst of the owl, and discussed above, have proved to be strikingly similar to those found in early visual cortical areas of carnivores and primates, in particular with respect to V1. However, when compared with most other birds or reptiles, this functional analogy between owls and mammals appears quite atypical, suggesting that it is probably due not to common ancestry but to independent evolution (Pettigrew, 1979; Shimizu & Bowers, 1999; Medina & Reiner, 2000). This hypothesis is also supported by developmental and anatomical evidence (Medina & Reiner, 2000). Thus, the owl visual system turns out to be an attractive experimental model to understand the fundamental question of how selective pressures have shaped the convergent or parallel evolution of modern amniotes' brains.

With this comparative perspective in mind, we deliberately followed methods commonly used in previous reports that have investigated the neural basis of motion perception in the visual cortex. To start with, we classified 66% of neurones in the owl visual wulst as directionally selective by adopting a DI threshold value of 0.5, thereby making the *a priori* assumption that the response strength of a direction-selective cell was at least two times greater in its preferred direction than in its antipreferred direction. Although to some extent arbitrary, this threshold value has been widely used to determine the directional selectivity of neurones in the visual cortex and is therefore adequate for comparative purposes.

In terms of the overall proportion of direction-selective cells, and keeping stimuli and classification criteria alike, our results closely match those found in V1 of cats, where most reported values range somewhere between 60 and 75% (Hamilton *et al.*, 1989; Gizzi *et al.*, 1990; Humphrey & Saul, 1998; Carandini & Ferster, 2000; Peterson *et al.*, 2004). Lower percentage values have been found in monkey V1 (20–50%) (De Valois *et al.*, 1982, 2000; Hawken *et al.*, 1988; Hamilton *et al.*, 1989; Snodderly & Gur, 1995; Movshon & Newsome, 1996; O'Keefe *et al.*, 1998; Tinsley *et al.*, 2003; Guo *et al.*, 2004; Gur *et al.*, 2005). However, this discrepancy diminishes if one considers that, in the latter, direction-selective cells are known to be mainly concentrated in layers 4b and 6, where such cells reach proportions of up to 70% (Schiller *et al.*, 1976; Hawken *et al.*, 1988; Snodderly & Gur, 1995; O'Keefe *et al.*, 1998; Gur *et al.*, 2005). As discussed earlier, the distribution of direction-selective cells is probably also layer-specific in the owl wulst and, accordingly, the latter would be more proximate to the striate cortex of the monkey than that of the cat. Anyway, it is clear that the representation of directional selectivity is less expressive in the wulst than in visual cortical areas highly specialized for motion processing, such as area MT in monkeys. In this area, for example, the average number of direction-selective cells is typically around 90% (Maunsell & van Essen, 1983; Albright, 1984; Felleman & Kaas, 1984; Rodman & Albright, 1987; Movshon & Newsome, 1996; Diogo *et al.*, 2003).

Our data on directional tuning bandwidths further support the notion of a close resemblance between the visual wulst and V1. Our population average for this band-pass characteristic was 28°. Similarly, in the V1 of both monkeys and cats, tuning bandwidths have been reported to range from 20° to 40° (Campbell *et al.*, 1968; Rose & Blakemore, 1974; Schiller *et al.*, 1976; De Valois *et al.*, 1982; Gizzi *et al.*, 1990; O'Keefe *et al.*, 1998; Carandini & Ferster, 2000; Gur *et al.*, 2005). Interestingly, the above-mentioned studies that used drifting sinusoidal gratings as stimuli had the closest results to our own. Again, figures in the wulst are quite different from those reported in area MT, where bandwidth estimates are on average twice as broad as those found in V1 and are more widely distributed (Maunsell & van Essen, 1983; Albright, 1984; Felleman & Kaas, 1984; Rodman & Albright, 1987; Lagae *et al.*, 1993; Britten & Newsome, 1998; Diogo *et al.*, 2003).

Motion integration

In response to plaid patterns, 80% of the direction-selective neurones in our sample were classified as CDS, none as PDS and 20% were unclassifiable. This distribution is, on the whole, strikingly similar to what has been described in the striate cortex of anaesthetized cats and monkeys (Movshon *et al.*, 1985; Gizzi *et al.*, 1990; Movshon & Newsome, 1996; Tinsley *et al.*, 2003; Guo *et al.*, 2004). The recent report by Guo *et al.* (2004) found that the incidence of pattern-selective cells was slightly higher in awake monkeys and speculated that this may be due to state-dependent feedback influences from extrastriate areas, MT in particular, on V1 cells. The lack of evidence for pattern selectivity in our study is solely based on experiments with animals that were awake and not actively engaged in a perceptual task related to the stimulus. Although this is also the case in Guo *et al.* (2004), it is still difficult to draw any conclusions about the non-existence of such feedback mechanisms in the owl. Moreover, although several visual areas project to the wulst (see Wild & Williams, 1999; Deng & Rogers, 2000), the paucity of available information concerning their functional properties does not permit, at the present stage, any conclusions about a hierarchical organization of the owl thalamofugal pathway at the level of the forebrain. In any case, the above considerations do not invalidate the two main points suggested by our results. First, like V1, the wulst seems to be the first stage of the thalamofugal pathway where directional selectivity is elaborated. Second, neurones in both of these areas signalize moving orientated contours instead of global motion.

In primates, converging evidence from anatomical, physiological and lesion studies suggests that increasingly complex motion computations take place along a parallel cortical pathway, which starts in V1 and heads towards the posterior parietal cortex (Andersen, 1997). In this pathway, area MT appears to play an important role in motion integration (Born & Bradley, 2005). To date, MT is in fact the only cortical area currently known in primates to have a considerable number of cells that responds to the global motion of plaids (roughly one-third) (Movshon *et al.*, 1985; Rodman & Albright, 1989; Movshon & Newsome, 1996; Pack *et al.*, 2001; Smith *et al.*, 2005). In cats, similar findings have been reported in regions of the lateral suprasylvian and ectosylvian cortices (Scannell *et al.*, 1996; Ouellette *et al.*, 2004). Although the exact mechanisms by which pattern motion selectivity emerges in those motion-specific areas still remain to be clarified (Majaj *et al.*, 2007), several lines of evidence indicate that they depend critically on inputs provided by CDS cells in V1 (Movshon *et al.*, 1985; Albright & Stoner, 1995). On the basis of such evidence, it has been proposed that V1 and MT might be the neural substrates for the first and second stages of global motion computation, respectively. According to this model, initial motion measurements are locally made by orientation-sensitive neurones, giving rise to the aperture problem. Signals from such neurones are then combined at a second stage to obtain a unified estimate of object motion, thereby solving the aperture problem for planar-translational motion. This two-stage processing scheme is also supported by a wealth of psychophysical data (e.g. Adelson & Movshon, 1982; Movshon *et al.*, 1985) and computer models (e.g. Simoncelli & Heeger, 1998; Rust *et al.*, 2006).

Given the overall functional similarities that we and others have found between V1 and the visual wulst of the owl, it is reasonable to speculate that the computation of global motion in the owl brain may be carried out by a pathway that includes the wulst as an initial processing stage. To validate this hypothesis, future investigations will clearly be needed to identify a candidate site for the explicit integration of the CDS signals provided by the wulst. The latter is known to project to a plethora of visual areas located both in and outside the telencephalon, several of them, such as, for example, the perientopallium, optic tectum and pretectum, containing motion-sensitive neurones (Karten *et al.*, 1973; Shimizu & Bowers, 1999; Deng, 2006). At present, any of these areas is a potential candidate, especially with regard to telencephalic areas, for which functional data are scarce if not non-existent. In the cat, Merabet *et al.* (1998) provided evidence that suggests that motion integration relies on distributed circuit dynamics, involving not only cortico-cortical connections but also cortico-thalamic loops. Considering that this could be the case in the owl, future investigations should therefore pay attention to possible large-scale circuits connecting intra- and extratelencephalic visual areas.

To date, the only study before ours that examined directional responses to plaid patterns in an avian brain was performed in two component nuclei of the pretectum and accessory optic system of the pigeon, namely the pretectal nucleus lentiformis mesencephali (LM) and the nucleus of the basal optic root (nBOR), respectively (Crowder & Wylie, 2002). Highly conserved in vertebrates, these two structures are involved with the analysis of optic flow resulting from self-motion and with the generation of compensatory motor behaviours like the optokinetic response that facilitates retinal image stabilization (for reviews see Simpson, 1984; Grasse & Cynader, 1990). There, neurones have typically large receptive fields in the contralateral hemifield and exhibit direction selectivity to wide-field moving stimuli (Morgan & Frost, 1981; Gioanni *et al.*, 1984; Winterson & Brauth, 1985; Wylie & Frost, 1990; Wylie & Crowder, 2000). Interestingly, in response to plaids, a majority of LM and nBOR neurones were found to be PDS ($\sim$ 50%) and only a few were CDS. In pigeons, telencephalic projections onto such neurones are restricted to the wulst (Wylie *et al.*, 2005). It has also been shown that electrical stimulation of the latter evokes excitatory activity in about one-third of LM (Crowder *et al.*, 2004) and nBOR (Nogueira & Britto, 1991) neurones. However, the question as to whether wulst inputs are important for the elaboration of pattern selectivity observed in these two nuclei remains unclear. Indeed, conflicting results have been reported regarding the degree to which such inputs actually contribute to the directional selectivity of LM and nBOR neurones. A pair of studies based on wulst ablation argues in favour (Hamassaki *et al.*, 1988; Britto *et al.*, 1990), whereas a more recent study, in which the wulst was temporarily inactivated with lidocaine, provides evidence against (Crowder *et al.*, 2004). Moreover, the fact that Crowder & Wylie (2002) found only a few CDS cells in both LM and nBOR suggests that orientation-sensitive signals, like those coming from the wulst, do not predominantly influence the neuronal responses in those

nuclei. As hypothesized by the authors, global motion selectivity in the pretectum and accessory optic system of the pigeon may be due to orientation-insensitive mechanisms, which involve the integration of retinal inputs, the major source of afferents to these nuclei. It would be interesting to investigate whether such a hypothesis also holds for owls, in which the wulst may have a greater influence on this brainstem visuomotor network, as suggested by the fact that nBOR neurones in the owl, unlike those in pigeons, are predominantly binocular (Wylie *et al.*, 1994).

Concluding remarks

To conclude, it is clear that much remains to be done in order to understand the neural basis of motion integration in the owl brain. Apart from its intrinsic value, this understanding will certainly also help to clarify the extent to which the thalamofugal pathway of the owl is functionally analogous to that of carnivores and primates. Several studies have reported that neurones in the upper part of the wulst encode some aspects of intermediate level vision that are usually attributed to extrastriate areas in mammals (Pettigrew, 1979; Nieder & Wagner, 1999, 2000; Liu & Pettigrew, 2003). Because of these findings, it has remained unclear whether a strict functional analogy between the visual wulst and striate cortex can be posited. At least in the specific domain of motion, our results reinforce the idea that the visual wulst can in fact be regarded as a primary visual forebrain area, very much like V1.

Acknowledgements

This work is dedicated to Jack Pettigrew who initially encouraged us to study this wonderful bird, the burrowing owl. We thank Karine Radd and Guilherme Lamego for assistance with some of the recordings, Nan-Hui Chen for the spike-sorting program, Danko Nikolić for the stimulus presentation software, and Mario Fiorani for advice on the head-fixation method. We also wish to thank Wolf Singer for his continuous support, Michaela Klinkmann for manufacturing the recording electrodes, Jacques Baron for assistance, and Rob van der Willigen for helpful comments on the manuscript. This work was funded by grants from the Research Support Foundation of the State of Minas Gerais (FAPEMIG, CBB-1018/04), the German/Brazilian Exchange Program (PROBRAL-CAPES-DAAD, D/03/23569), the Program for Centers of Excellence PRONEX (CNPq-FAPERJ, E26/171210/2003), and the FINEP research grant Rede Instituto Brasileiro de Neurociência (IBN-Net 01.06.0842-00). L. P. received a scholarship from the Brazilian National Council for Scientific and Technological Development (CNPq).

Abbreviations

CDS, component direction selective; DI, direction index; HA, hyperpallium apicale; LM, pretectal nucleus lentiformis mesencephali; MT, middle temporal area; nBOR, nucleus of the basal optic root; PDS, pattern direction selective; R_c, partial correlation coefficient for the component prediction; R_p, partial correlation coefficient for the pattern prediction; V1, primary visual cortex.

References

Adelson, E.H. & Movshon, J.A. (1982) Phenomenal coherence of moving visual patterns. *Nature*, **300**, 523–525.

Albright, T.D. (1984) Direction and orientation selectivity of neurons in visual area MT of the macaque. *J. Neurophysiol.*, **52**, 1106–1130.

Albright, T.D. (1989) Centrifugal directional bias in the middle temporal visual area (MT) of the macaque. *Vis. Neurosci.*, **2**, 177–188.

Albright, T.D. & Stoner, G.R. (1995) Visual motion perception. *Proc. Natl Acad. Sci. U.S.A.*, **92**, 2433–2440.

Andersen, R.A. (1997) Neural mechanisms of visual motion perception in primates. *Neuron*, **18**, 865–872.

Azzi, J.C.B. (2004) O mapa do córtex visual primário é visuotópico e não retinotópico: visuotopia do ponto cego em V1 de primatas (cebus apella). PhD Thesis. Universidade Federal do Rio de Janeiro.

Barlow, H.B., Blakemore, C. & Pettigrew, J.D. (1967) The neural mechanism of binocular depth discrimination. *J. Physiol.*, **193**, 327–342.

Blakemore, C. & Tobin, E.A. (1972) Lateral inhibition between orientation detectors in the cat's visual cortex. *Exp. Brain Res.*, **15**, 439–440.

Bonds, A.B. (1989) Role of inhibition in the specification of orientation selectivity of cells in the cat striate cortex. *Vis. Neurosci.*, **2**, 41–55.

Born, R.T. & Bradley, D.C. (2005) Structure and function of visual area MT. *Annu. Rev. Neurosci.*, **28**, 157–189.

Bradley, D.C., Qian, N. & Andersen, R.A. (1995) Integration of motion and stereopsis in middle temporal cortical area of macaques. *Nature*, **373**, 609–611.

Bradshaw, M.F. & Cumming, B.G. (1997) The direction of retinal motion facilitates binocular stereopsis. *Proc. Biol. Sci.*, **264**, 1421–1427.

Branch, M.A., Coleman, T.F. & Li, Y. (1999) A subspace, interior and conjugate gradient method for large-scale bound-constrained minimization problems. *SIAM J. Sci. Comput.*, **21**, 1–23.

Bravo, H. & Pettigrew, J.D. (1981) The distribution of neurons projecting from the retina and visual cortex to the thalamus and tectum opticum of the barn owl, Tyto alba, and the burrowing owl, Speotyto cunicularia. *J. Comp. Neurol.*, **199**, 419–441.

Britten, K.H. & Newsome, W.T. (1998) Tuning bandwidths for near-threshold stimuli in area MT. *J. Neurophysiol.*, **80**, 762–770.

Britto, L.R., Gasparotto, O.C. & Hamassaki, D.E. (1990) Visual telencephalon modulates directional selectivity of accessory optic neurons in pigeons. *Vis. Neurosci.*, **4**, 3–10.

Budzynski, C.A. & Bingman, V.P. (2004) Participation of the thalamofugal visual pathway in a coarse pattern discrimination task in an open arena. *Behav. Brain Res.*, **153**, 543–556.

Campbell, F.W., Cleland, B.G., Cooper, G.F. & Enroth-Cugell, C. (1968) The angular selectivity of visual cortical cells to moving gratings. *J. Physiol.*, **198**, 237–250.

Carandini, M. & Ferster, D. (2000) Membrane potential and firing rate in cat primary visual cortex. *J. Neurosci.*, **20**, 470–484.

Carpenter, G.A. & Grossberg, S. (1987) Discovering order in chaos: stable self-organization of neural recognition codes. *Ann. N.Y. Acad. Sci.*, **504**, 33–51.

Cooper, M.L. & Pettigrew, J.D. (1979) A neurophysiological determination of the vertical horopter in the cat and owl. *J. Comp. Neurol.*, **184**, 1–26.

Coulombe, H.N. (1971) Behavior and population ecology of the burrowing owl, *Speotyto cunicularia*, in the Imperial Valley of California. *Condor*, **73**, 162–176.

Crowder, N.A. & Wylie, D.R. (2002) Responses of optokinetic neurons in the pretectum and accessory optic system of the pigeon to large-field plaids. *J. Comp. Physiol. A Neuroethol. Sens. Neural Behav. Physiol.*, **188**, 109–119.

Crowder, N.A., Dickson, C.T. & Wylie, D.R. (2004) Telencephalic input to the pretectum of pigeons: an electrophysiological and pharmacological inactivation study. *J. Neurophysiol.*, **91**, 274–285.

DeAngelis, G.C., Robson, J.G., Ohzawa, I. & Freeman, R.D. (1992) Organization of suppression in receptive fields of neurons in cat visual cortex. *J. Neurophysiol.*, **68**, 144–163.

De Britto, L.R., Brunelli, M., Francesconi, W. & Magni, F. (1975) Visual response pattern of thalamic neurons in the pigeon. *Brain Res.*, **97**, 337–343.

Deng, C. (2006) Relative contributions of the two visual pathways to avian behavior. *Acta Zool. Sin.*, **52** (Suppl.), 379–383.

Deng, C. & Rogers, L.J. (2000) Organization of intratelencephalic projections to the visual Wulst of the chick. *Brain Res.*, **856**, 152–162.

De Valois, R.L., Albrecht, D.G. & Thorell, L.G. (1982) Spatial frequency selectivity of cells in macaque visual cortex. *Vis. Res.*, **22**, 545–559.

De Valois, R.L., Cottaris, N.P., Mahon, L.E., Elfar, S.D. & Wilson, J.A. (2000) Spatial and temporal receptive fields of geniculate and cortical cells and directional selectivity. *Vis. Res.*, **40**, 3685–3702.

Diogo, A.C., Soares, J.G., Koulakov, A., Albright, T.D. & Gattass, R. (2003) Electrophysiological imaging of functional architecture in the cortical middle temporal visual area of Cebus apella monkey. *J. Neurosci.*, **23**, 3881–3898.

Felleman, D.J. & Kaas, J.H. (1984) Receptive-field properties of neurons in middle temporal visual area (MT) of owl monkeys. *J. Neurophysiol.*, **52**, 488–513.

Fennema, C. & Thompson, W.B. (1979) Velocity determination in scenes containing several moving images. *Comput. Graph. Image Proc.*, **9**, 301–315.

Ferster, D. (2004) Assembly of receptive fields in primary visual cortex. In Chalupa, L.M. & Werner, J.S. (Eds), *The Visual Neurosciences*. A Bradford Book. MIT Press, Cambridge, MA, pp. 695–703.
Gioanni, H., Rey, J., Villalobos, J. & Dalbera, A. (1984) Single unit activity in the nucleus of the basal optic root (nBOR) during optokinetic, vestibular and visuo-vestibular stimulations in the alert pigeon (Columbia livia). *Exp. Brain Res.*, **57**, 49–60.
Gizzi, M.S., Katz, E., Schumer, R.A. & Movshon, J.A. (1990) Selectivity for orientation and direction of motion of single neurons in cat striate and extrastriate visual cortex. *J. Neurophysiol.*, **63**, 1529–1543.
Grasse, K.L. & Cynader, M.S. (1990) The accessory optic system in frontal-eyed animals. In Leventhal, A. (Ed.), *Vision and Visual Dysfunction.* McMillan, New York, pp. 111–139.
Guo, K., Benson, P.J. & Blakemore, C. (2004) Pattern motion is present in V1 of awake but not anaesthetized monkeys. *Eur. J. Neurosci.*, **19**, 1055–1066.
Gur, M., Kagan, I. & Snodderly, D.M. (2005) Orientation and direction selectivity of neurons in V1 of alert monkeys. functional relationships and laminar distributions. *Cereb. Cortex*, **15**, 1207–1221.
Hahmann, U. & Güntürkün, O. (1993) The visual acuity for the lateral visual field of the pigeon (Columba livia). *Vis. Res.*, **33**, 1659–1664.
Hamassaki, D.E., Gasparotto, O.C., Nogueira, M.I. & Britto, L.R. (1988) Telencephalic and pretectal modulation of the directional selectivity of accessory optic neurons in the pigeon. *Braz. J. Med. Biol. Res.*, **21**, 649–652.
Hamilton, D.B., Albrecht, D.G. & Geisler, W.S. (1989) Visual cortical receptive fields in monkey and cat: spatial and temporal phase transfer function. *Vis. Res.*, **29**, 1285–1308.
Hawken, M.J., Parker, A.J. & Lund, J.S. (1988) Laminar organization and contrast sensitivity of direction-selective cells in the striate cortex of the Old World monkey. *J. Neurosci.*, **8**, 3541–3548.
Henry, G.H., Bishop, P.O. & Dreher, B. (1974) Orientation, axis and direction as stimulus parameters for striate cells. *Vis. Res.*, **14**, 767–777.
Hubel, D.H. & Wiesel, T.N. (1962) Receptive fields, binocular interaction and functional architecture in the cat's visual cortex. *J. Physiol.*, **160**, 106–154.
Hubel, D.H. & Wiesel, T.N. (1968) Receptive fields and functional architecture of monkey striate cortex. *J. Physiol.*, **195**, 215–243.
Humphrey, A.L. & Saul, A.B. (1998) Strobe rearing reduces direction selectivity in area 17 by altering spatiotemporal receptive-field structure. *J. Neurophysiol.*, **80**, 2991–3004.
Iwaniuk, A.N. & Hurd, P.L. (2005) The evolution of cerebrotypes in birds. *Brain Behav. Evol.*, **65**, 215–230.
Iwaniuk, A.N. & Wylie, D.R. (2006) The evolution of stereopsis and the Wulst in caprimulgiform birds: a comparative analysis. *J. Comp. Physiol. A Neuroethol. Sens. Neural Behav. Physiol.*, **192**, 1313–1326.
Jassik-Gerschenfeld, D., Teulon, J. & Ropert, N. (1976) Visual receptive field types in the nucleus dorsolateralis anterior of the pigeon's thalamus. *Brain Res.*, **108**, 295–306.
Karten, H.J., Hodos, W., Nauta, W.J. & Revzin, A.M. (1973) Neural connections of the 'visual wulst' of the avian telencephalon. Experimental studies in the pigeon (Columba livia) and owl (Speotyto cunicularia). *J. Comp. Neurol.*, **150**, 253–278.
Knudsen, E.I. (1982) Auditory and visual maps of space in the optic tectum of the owl. *J. Neurosci.*, **2**, 1177–1194.
Konishi, M. (1993) Listening with two ears. *Sci. Am.*, **268**, 66–73.
Lagae, L., Raiguel, S. & Orban, G.A. (1993) Speed and direction selectivity of macaque middle temporal neurons. *J. Neurophysiol.*, **69**, 19–39.
Liu, G.B. & Pettigrew, J.D. (2003) Orientation mosaic in barn owl's visual Wulst revealed by optical imaging: comparison with cat and monkey striate and extra-striate areas. *Brain Res.*, **961**, 153–158.
Majaj, N.J., Carandini, M. & Movshon, J.A. (2007) Motion integration by neurons in macaque MT is local, not global. *J. Neurosci.*, **27**, 366–370.
Marr, D. & Ullman, S. (1981) Directional selectivity and its use in early visual processing. *Proc. R. Soc. Lond. B Biol. Sci.*, **211**, 151–180.
Martin, G.R. (1984) The visual fields of the tawny owl, Strix aluco L. *Vis. Res.*, **24**, 1739–1751.
Maunsell, J.H. & van Essen, D.C. (1983) Functional properties of neurons in middle temporal visual area of the macaque monkey. I. Selectivity for stimulus direction, speed, and orientation. *J. Neurophysiol.*, **49**, 1127–1147.
Medina, L. & Reiner, A. (2000) Do birds possess homologues of mammalian primary visual, somatosensory and motor cortices? *Trends Neurosci.*, **23**, 1–12.
Merabet, L., Desautels, A., Minville, K. & Casanova, C. (1998) Motion integration in a thalamic visual nucleus. *Nature*, **396**, 265–268.
Miceli, D., Gioanni, H., Reperant, J. & Peyrichou, J. (1979) The avian visual wulst. I. An anatomical study of afferent and efferent pathways. II. An electrophysiological study of the functional properties of single neurons. In Granada, A.M. & Maxwell, J.H. (Eds), *Neural Mechanisms of Behavior in the Pigeon*. Plenum Press, New York, pp. 223–254.
Morgan, B. & Frost, B.J. (1981) Visual response characteristics of neurons in nucleus of basal optic root of pigeons. *Exp. Brain Res.*, **42**, 181–188.
Morrone, M.C., Burr, D.C. & Maffei, L. (1982) Functional implications of cross-orientation inhibition of cortical visual cells. I. Neurophysiological evidence. *Proc. R. Soc. Lond. B Biol. Sci.*, **216**, 335–354.
Movshon, J.A. & Newsome, W.T. (1996) Visual response properties of striate cortical neurons projecting to area MT in macaque monkeys. *J. Neurosci.*, **16**, 7733–7741.
Movshon, J.A., Adelson, E.H., Gizzi, M.S. & Newsome, W.T. (1985) The analysis of moving visual patterns. In Chagas, C., Gattass, R. & Gross, C. (Eds), *Study Week on Pattern Recognition Mechanisms. Pont. Acad. Scient. Scrip. Varta*. Vatican Press, Vatican City, **Vol. 54**, pp. 117–151.
Nieder, A. & Wagner, H. (1999) Perception and neuronal coding of subjective contours in the owl. *Nat. Neurosci.*, **2**, 660–663.
Nieder, A. & Wagner, H. (2000) Horizontal-disparity tuning of neurons in the visual forebrain of the behaving barn owl. *J. Neurophysiol.*, **83**, 2967–2979.
Nieder, A. & Wagner, H. (2001a) Encoding of both vertical and horizontal disparity in random-dot stereograms by Wulst neurons of awake barn owls. *Vis. Neurosci.*, **18**, 541–547.
Nieder, A. & Wagner, H. (2001b) Hierarchical processing of horizontal disparity information in the visual forebrain of behaving owls. *J. Neurosci.*, **21**, 4514–4522.
Niu, Y.Q., Xiao, Q., Liu, R.F., Wu, L.Q. & Wang, S.R. (2006) Response characteristics of the pigeon's pretectal neurons to illusory contours and motion. *J. Physiol.*, **577**, 805–813.
Nogueira, M.I. & Britto, L.R. (1991) Extraretinal modulation of accessory optic units in the pigeon. *Braz. J. Med. Biol. Res.*, **24**, 623–631.
Norberg, R.A. (1977) Ocurrence and independent evolution of bilateral ear assymetry in owls and implication in owl taxonomy. *Philos. Trans. R. Soc. Lond. Ser. B*, **280**, 375–408.
O'Keefe, L.P., Levitt, J.B., Kiper, D.C., Shapley, R.M. & Movshon, J.A. (1998) Functional organization of owl monkey lateral geniculate nucleus and visual cortex. *J. Neurophysiol.*, **80**, 594–609.
Ouellette, B.G., Minville, K., Faubert, J. & Casanova, C. (2004) Simple and complex visual motion response properties in the anterior medial bank of the lateral suprasylvian cortex. *Neuroscience*, **123**, 231–245.
Pack, C.C., Berezovskii, V.K. & Born, R.T. (2001) Dynamic properties of neurons in cortical area MT in alert and anaesthetized macaque monkeys. *Nature*, **414**, 905–908.
Papoulis, A. (1990) *Probability and Statistics*. Prentice Hall, Englewood Cliffs, NJ.
Pateromichelakis, S. (1981) Response properties of visual units in the anterior dorsolateral thalamus of the chick (Gallus domesticus). *Experientia*, **37**, 279–280.
Peterson, M.R., Li, B. & Freeman, R.D. (2004) The derivation of direction selectivity in the striate cortex. *J. Neurosci.*, **24**, 3583–3591.
Pettigrew, J.D. (1979) Binocular visual processing in the owl's telencephalon. *Proc. R. Soc. Lond.*, **204**, 435–454.
Pettigrew, J.D. & Konishi, M. (1976) Neurons selective for orientation and binocular disparity in the visual Wulst of the barn owl (Tyto alba). *Science*, **193**, 675–678.
Pinto, L., Dias, M.O., Lima, B., Neuenschwander, S. & Baron, J. (2006) Response of visual Wulst neurons to plaid patterns in the burrowing owl. In *XXI Reunião Anual Da Federação de Sociedades Brasileiras de Biologia Experimental-FeSBE 2006*, Águas de Lindúia, no. 05.125.
Pinto, L., Dias, M.O., Lima, B., Neuenschwander, S. & Baron, J. (2007) Steady-state and dynamical aspects of component direction selectivity in the visual Wulst of awake owls. In *II International Neurosciences Symposium of the IINN*, Natal, No. 156.
Reiner, A., Perkel, D.J., Bruce, L.L., Butler, A.B., Csillag, A., Kuenzel, W., Medina, L., Paxinos, G., Shimizu, T., Striedter, G., Wild, M., Ball, G.F., Durand, S., Gunturkun, O., Lee, D.W., Mello, C.V., Powers, A., White, S.A., Hough, G., Kubikova, L., Smulders, T.V., Wada, K., Dugas-Ford, J., Husband, S., Yamamoto, K., Yu, J., Siang, C. & Jarvis, E.D. (2004) Revised nomenclature for avian telencephalon and some related brainstem nuclei. *J. Comp. Neurol.*, **473**, 377–414.
Richards, W. (1985) Structure from stereo and motion. *J. Opt. Soc. Am. [A]*, **2**, 343–349.
Rodman, H.R. & Albright, T.D. (1987) Coding of visual stimulus velocity in area MT of the macaque. *Vis. Res.*, **27**, 2035–2048.
Rodman, H.R. & Albright, T.D. (1989) Single-unit analysis of pattern-motion selective properties in the middle temporal visual area (MT). *Exp. Brain Res.*, **75**, 53–64.

Rogers, B.J. & Collett, T.S. (1989) The appearance of surfaces specified by motion parallax and binocular disparity. *Q. J. Exp. Psychol. A*, **41**, 697–717.
Rose, D. & Blakemore, C. (1974) An analysis of orientation selectivity in the cat's visual cortex. *Exp. Brain Res.*, **20**, 1–17.
Rust, N.C., Mante, V., Simoncelli, E.P. & Movshon, J.A. (2006) How MT cells analyze the motion of visual patterns. *Nat. Neurosci.*, **9**, 1421–1431.
Scannell, J.W., Sengpiel, F., Tovee, M.J., Benson, P.J., Blakemore, C. & Young, M.P. (1996) Visual motion processing in the anterior ectosylvian sulcus of the cat. *J. Neurophysiol.*, **76**, 895–907.
Schiller, P.H., Finlay, B.L. & Volman, S.F. (1976) Quantitative studies of single-cell properties in monkey striate cortex. II. Orientation specificity and ocular dominance. *J. Neurophysiol.*, **39**, 1320–1333.
Shimizu, T. & Bowers, A.N. (1999) Visual circuits of the avian telencephalon: evolutionary implications. *Behav. Brain Res.*, **98**, 183–191.
Simoncelli, E.P. & Heeger, D.J. (1998) A model of neuronal responses in visual area MT. *Vis. Res.*, **38**, 743–761.
Simpson, J.I. (1984) The accessory optic system. *Annu. Rev. Neurosci.*, **7**, 13–41.
Singer, W. (2004) Synchrony, oscillations and relational codes. In Chalupa, L.M. & Werner, J.S. (Eds), *The Visual Neurosciences*. A Bradford Book. MIT Press, Cambridge, MA, pp. 1665–1681.
Smith, M.A., Majaj, N.J. & Movshon, J.A. (2005) Dynamics of motion signaling by neurons in macaque area MT. *Nat. Neurosci.*, **8**, 220–228.
Snodderly, D.M. & Gur, M. (1995) Organization of striate cortex of alert, trained monkeys (Macaca fascicularis): ongoing activity, stimulus selectivity, and widths of receptive field activating regions. *J. Neurophysiol.*, **74**, 2100–2125.
Spath, H. (1980) *Cluster Analysis Algorithims for Reduction and Classification of Objects*. Ellis Horwood, West Sussex, UK.
Steinbach, M.J., Angus, R.G. & Money, K.E. (1974) Torsional eye movements of the owl. *Vis. Res.*, **14**, 745–746.
Stingelin, W. (1958) Vergleichend-morphologische Untersuchungen am Vorderhirn der Vögel auf cytologischer und cytoarchitektonischer Grundlage. Helbing & Lichtenhahn, Basel, Switzerland.
Stoner, G.R. & Albright, T.D. (1992) Neural correlates of perceptual motion coherence. *Nature*, **358**, 412–414.
Swindale, N.V., Grinvald, A. & Shmuel, A. (2003) The spatial pattern of response magnitude and selectivity for orientation and direction in cat visual cortex. *Cereb. Cortex*, **13**, 225–238.
Tinsley, C.J., Webb, B.S., Barraclough, N.E., Vincent, C.J., Parker, A. & Derrington, A.M. (2003) The nature of V1 neural responses to 2D moving patterns depends on receptive-field structure in the marmoset monkey. *J. Neurophysiol.*, **90**, 930–937.
Wagner, H. & Frost, B. (1993) Disparity-sensitive cells in the owl have a characteristic disparity. *Nature*, **364**, 796–798.
Wagner, H. & Frost, B. (1994) Binocular responses of neurons in the barn owl's visual wulst. *J. Comp. Physiol. A*, **174**, 661–670.
Wallach, H. (1935) Über visuell wahrgenommene Bewegungsrichtung. *Psychol. Forsch.*, **20**, 325–380.
van Wezel, R.J. & van der Smagt, M.J. (2003) Motion processing: how low can you go? *Curr. Biol.*, **13**, R840–R842.
Wheeler, B.C. (1999) Automatic discrimination of single units. In Nicolelis, M.A.L. (Ed.), *Methods of Neural Ensemble Recording*. Methods in Life Sciences. CRC Press, Boca Raton, FL, pp. 61–78.
Wild, J.M. & Williams, M.N. (1999) Rostral wulst of passerine birds. II. Intratelencephalic projections to nuclei associated with the auditory and song systems. *J. Comp. Neurol.*, **413**, 520–534.
van der Willigen, R.F., Frost, B.J. & Wagner, H. (1998) Stereoscopic depth perception in the owl. *Neuroreport*, **9**, 1233–1237.
van der Willigen, R.F., Frost, B.J. & Wagner, H. (2002) Depth generalization from stereo to motion parallax in the owl. *J. Comp. Physiol. A Neuroethol. Sens. Neural Behav. Physiol.*, **187**, 997–1007.
van der Willigen, R.F., Frost, B.J. & Wagner, H. (2003) How owls structure visual information. *Anim. Cogn.*, **6**, 39–55.
Wilson, P. (1980a) The organization of the visual hyperstriatum in the domestic chick. II. Receptive field properties of single units. *Brain Res.*, **188**, 333–345.
Wilson, P. (1980b) The organization of the visual hyperstriatum in the domestic chick. I. Topology and topography of the visual projection. *Brain Res.*, **188**, 319–332.
Winterson, B.J. & Brauth, S.E. (1985) Direction-selective single units in the nucleus lentiformis mesencephali of the pigeon (Columba livia). *Exp. Brain Res.*, **60**, 215–226.
Wörgötter, F., Niebur, E. & Koch, C. (1991) Isotropic connections generate functional asymmetrical behavior in visual cortical cells. *J. Neurophysiol.*, **66**, 444–459.
Wylie, D.R. & Crowder, N.A. (2000) Spatiotemporal properties of fast and slow neurons in the pretectal nucleus lentiformis mesencephali in pigeons. *J. Neurophysiol.*, **84**, 2529–2540.
Wylie, D.R. & Frost, B.J. (1990) The visual response properties of neurons in the nucleus of the basal optic root of the pigeon: a quantitative analysis. *Exp. Brain Res.*, **82**, 327–336.
Wylie, D.R., Shaver, S.W. & Frost, B.J. (1994) The visual response properties of neurons in the nucleus of the basal optic root of the northern saw-whet owl (Aegolius acadicus). *Brain Behav. Evol.*, **43**, 15–25.
Wylie, D.R., Ogilvie, C.J., Crowder, N.A., Barkley, R.R. & Winship, I.R. (2005) Telencephalic projections to the nucleus of the basal optic root and pretectal nucleus lentiformis mesencephali in pigeons. *Vis. Neurosci.*, **22**, 237–247.